

Can reverberation-measured quasars be used for cosmology?

MARY LOLI MARTÍNEZ-ALDAMA,¹ BOŻENA CZERNY,¹ DAMIAN KAWKA,¹ VLADIMÍR KARAS,² MICHAL ZAJAČEK,¹ AND PIOTR T. ŹYCKI³

¹*Center for Theoretical Physics, Polish Academy of Sciences, Al. Lotników 32/46, 02-668 Warsaw, Poland*

²*Astronomical Institute, Academy of Sciences, Bocni II, CZ-141 31 Prague, Czech Republic*

³*Copernicus Astronomical Center, Polish Academy of Sciences, ul. Bartycka 18, 00-716 Warsaw, Poland*

(Received XXXX XX, 2019; Revised XXXX XX, 2019; Accepted XXXX XX, 2019)

Submitted to ApJ

ABSTRACT

Quasars have been proposed as a new class of standard candles analogous to Supernovae, as their large redshift range and high luminosities make them excellent candidates. Reverberation mapping (RM) method enables to estimate the distance to the source from the time delay measurement of the emission lines with respect to the continuum, since the time delay depends on the absolute luminosity of the source. This radius-luminosity (RL) relation exhibits a low scatter and it was thus proposed for the cosmological purposes. However, in the recent years the increase in the studied sample, and in particular the inclusion of highly accreting QSO has increased the dispersion in the RL relation, with many objects showing time delays shorter than the expected. Using $\text{H}\beta$ RM measurements for 117 sources with $0.2 < z < 0.9$ and $41.5 < \log L_{5100} < 45.9$, we find a correction for the time delay based on the dimensionless accretion rate (\dot{M}) considering the virial factor anti-correlated with the FWHM of $\text{H}\beta$. This correction decreases the scattering in the accretion parameters compared with typical value used, which is directly reflected by suppressing the RL relation dispersion. We also confirm the anti-correlation between the excess of variability and the accretion parameters. With this correction we are able to build the Hubble diagram and estimate the cosmological constants Ω_m and Ω_Λ , which are consistent with standard cosmological model at 2σ confidence level. Therefore, RM results can be used to constrain cosmological models in the future.

Keywords: galaxies: active – quasars: emission lines – reverberation mapping – cosmology

1. INTRODUCTION

Understanding dark energy is one of the greatest puzzles of the modern physics. In order to test numerous theories proposed to explain the phenomenon of accelerated expansion of the Universe, we first need to measure it precisely. There are well-established methods such as the studies of the Cosmic Microwave Background, Supernovae Ia (SNIa), Baryon Acoustic Oscillations, and weak lensing. Combination of these method currently brings the following cosmological parameters: $H_0 = 67.66 \pm 0.42 \text{ km s}^{-1} \text{ Mpc}^{-1}$, $\Omega_\Lambda = 0.6889 \pm 0.0056$, $\Omega_m = 0.3111 \pm 0.0056$ (Planck Collaboration 2018). These results are consistent with the simplest interpretation of the cosmological constant in dark

matter dominated Universe in the form of Λ cold dark matter model (Planck Collaboration 2016a). However, there is some tension now with the local measurements of the Hubble constant (Riess et al. 2018), amplitude of matter fluctuations in the late time Universe compared to cosmic shear measurements (Joudaki et al. 2017; Hildebrandt et al. 2017), and the number counts of galaxy clusters (Planck Collaboration (2016b); see Pacaud et al. (2018) for most recent results). Therefore, new objects are proposed as tools constrain better the Universe expansion, and active galactic nuclei (AGN) are among them (e.g. Czerny et al. 2018).

AGN cover a broad range of redshift, and they do not show strong evolution with the redshift – even for example, the most distant quasars have metallicities similar to the nearby AGN (close to the solar value, or slightly higher (e.g. Groves et al. 2006). This could be caused by the combination of efficient rotational mixing and powerful stellar winds of early massive stars (Maeder & Meynet 2000; Brott et al. 2011; Ek-

ström et al. 2012), which could transport the heavier nucleosynthesis products to the surface of massive stars already within ~ 10 Myr of the stellar evolution (Stanway & Eldridge 2019). Powerful stellar winds would further enrich the ISM of early quasars.

Reverberation campaigns revealed a very strong and tight correlation between the broad line region (BLR) size and the monochromatic luminosity at 5100Å, producing the well-known radius-luminosity relation, $R_{\text{H}\beta} - L_{5100}$ (Kaspi et al. 2000; Peterson et al. 2004; Bentz et al. 2013). Such a relation offers prospects of cosmological applications. After proper calibration, the time delay measurement allows us to determine the absolute luminosity, and to use a generalized standard candle approach to obtain the cosmological parameters (Watson et al. 2011; Haas et al. 2011; Czerny et al. 2013; King & Lasota 2014).

The problem has started with the detection of some outliers from the radius-luminosity relation Bentz et al. (2013). First, outliers from the $R_{\text{H}\beta} - L_{5100}$ relation have been found among the highly super-Eddington sources which were the subject of the super-Eddington accreting massive black holes (SEAMBHs) campaign (Du et al. 2014; Wang et al. 2014c; Hu et al. 2015; Du et al. 2015, 2016, 2018). The interpretation is that the measured delays much shorter than implied by the standard $R_{\text{H}\beta} - L_{5100}$ relation (Bentz et al. 2013) are caused by the self-shielding of geometrically thick accretion disk which subsequently modifies the radiation field seen by the surrounding material forming the BLR (Wang et al. 2014b).

Recently, more sources with considerably shorter than expected time delays were found by Grier et al. (2017) and Du et al. (2018). A significant fraction of them have low values of the Eddington ratio, and they cannot be simply eliminated from the sample. If the $R_{\text{H}\beta} - L_{5100}$ relation has such a large scatter, application of AGN to cosmology based on this relation is problematic, unless we understand what additional parameter is responsible for the departure from the original $R_{\text{H}\beta} - L_{5100}$ relation, and are able to correct for this trend. It poses also a question about the nature of the standard radius-luminosity relation and the physical reasons for the departures from this law. These shortened lags could be explained for example by retrograde accretion (Wang et al. 2014a; Du et al. 2018), the inner disk evaporation, or replacing the dust-based model of BLR formation (Czerny & Hryniwicz 2011; Czerny et al. 2015, 2017) with the old model based on assumption of ampleness of gaseous material close to the nucleus and formation of the BLR where the ionization parameter has the optimum value (Czerny et al. 2019).

In this paper we analyze in detail how the properties of active galaxies correlate with their location with respect to the standard $R_{\text{H}\beta} - L_{5100}$ relation. Section 2 gives a description of the different $\text{H}\beta$ reverberated-measured sub-

samples considered in this work and the relations used to estimate the main physical parameters, such as virial factor, black hole mass, accretion parameters, variability, etc. Section 3 describes the correction for the time delay based on the accretion parameters recovering the low scattering along the $R_{\text{H}\beta} - L_{5100}$ relation. We confirm the anti-correlation between the variability and the accretion parameters as well. Section 4 presents the Hubble diagram built with the reverberated-measured sample and the possible cosmological implications. In section 5, we review the main result of this work. Absolute values of the luminosity are given assuming the cosmological parameters: $H_0 = 67 \text{ km s}^{-1} \text{ Mpc}^{-1}$, $\Omega_\Lambda = 0.68$, $\Omega_m = 0.32$ (Planck Collaboration 2013).

2. METHOD

2.1. Observational data

Our sample of $\text{H}\beta$ reverberation-measured AGN is a compilation of the results published earlier in the literature. It was previously used by Czerny et al. (2019): luminosity (L_{5100}), time delay (τ_{obs}) and FWHM are the same as considered by them. We have collected a total of 117 sources, plus 2 objects which have been discarded from the analysis (see details in section 2.2). The first sub-sample is composed by 25 high accretion rate AGN observed by the SEAMBH (Super-Eddington Accretion in Massive Black Holes) project (Du et al. 2014; Wang et al. 2014c; Hu et al. 2015; Du et al. 2015, 2016, 2018). SEAMBH project group have been monitoring super-Eddington sources since 2012 obtaining important results for this kind of objects. The second sub-sample contains 44 objects from the recent SDSS-RM (Sloan Digital Sky Survey Reverberation Measurement) project (Grier et al. 2017); two sources of this sample have been discarded. This sample comes from a larger sample of Shen et al. (2015), recently they have published an update of the catalog with additional information such as the variability properties (Shen et al. 2018). The third sub-sample is a collection of 48 sources from a long-term monitoring projects, where the majority of the sources have been summarized by Bentz et al. (2013). We include in this sample other sources monitored in the recent years (Bentz et al. 2009, 2014; Barth et al. 2013; Pei et al. 2014; Bentz et al. 2016a,b; Fausnaugh et al. 2017). The fourth sub-sample includes NGC 5548 and 3C 273 (PG 1226+023) monitored by Lu et al. (2016) and Zhang et al. (2018), respectively. 3C 273 was previously monitored by Kaspi et al. (2000) and Peterson et al. (2004), however new results from GRAVITY Collaboration (Gravity Collaboration et al. 2018) resolved the BLR with a much better angular resolution of $10^{-5}''$ indicating a smaller BLR size (~ 150 light days) than the reverberation mapping results. Also, the BLR size for 3C 273 reported by Zhang et al. (2018) is simi-

lar to the one given by [Gravity Collaboration et al. \(2018\)](#), so we will use the new estimation.

These sources do not form a uniform sample. Sources from the Bentz Collection were selected to cover broad range of redshift ($0.002 \lesssim z \lesssim 0.292$), from nearby sources studied earlier for example by [Peterson et al. \(2004\)](#) to more distant PG quasar sample from [Kaspi et al. \(2000\)](#). The average luminosity and dimensionless accretion rate are $\log L_{5100} = 43.4$ erg s $^{-1}$ and $\dot{M}^c \sim 0.8$ (See section 2.3), respectively. Sources from SDSS-RM sample are on average slightly more luminous, $\log L_{5100} = 43.9$ erg s $^{-1}$, and cover systematically larger redshifts, $0.116 \lesssim z \lesssim 0.89$. On the other hand, SEAMBH sample has been selected with the aim to study super-Eddington sources, they are nearby objects ($0.017 \lesssim z \lesssim 0.4$), but with the largest accretion rates, $\dot{M}^c_{mean} \sim 14.6$ (See section 2.3).

The full sample includes 117 sources and covers a large redshift range ($0.002 \lesssim z \lesssim 0.89$), which is convenient in order to test cosmological models. A detail description of the sample is shown in Table 1.

2.2. Discarded objects, and biases in the sample

Two objects from SDSS-RM sample have been discarded from the analysis: J141856 and J141314. In the case of J141856 there is no detection of the blue side of H β line, destroying the profile and prohibiting any possibility of measurement. In J141314 the H β line is at the border of the spectrum, where the S/N is poor and the emission line cannot be observed.

Observational problems can cause an incorrect estimation in the time delay, see Section 3.2 and Appendix A. It is important to stress that $\sim 30\%$ of the SDSS-RM sample has a contribution of the host galaxy luminosity $> 50\%$ with respect to AGN. In order to decompose the quasar and host-galaxy contribution, [Shen et al. \(2015\)](#) applied a principal component analysis (PCA). This method could present some systematic uncertainties in the decomposition, due to the limited S/N or insufficient host contribution. However, in all the analyzed cases PCA is successful decomposing both components, even those where S/N and the equivalent width are low, e.g. J141123.

In addition, some objects from the Bentz collection show a large variability that could change significantly the time delay. For example, the H β broad component in NGC5548 seems to appear and disappear over the years (e.g. [Sergeev et al. 2007](#)). However, variations in the measurements seem to be included in the intrinsic scatter of the $R_{H\beta} - L_{5100}$ relation ([Kilerci Eser et al. 2015](#)). Therefore, any possible deviation from $R_{H\beta} - L_{5100}$ relation could not be attributed to the variability of the object itself.

2.3. Black hole mass and accretion parameters

Some of the sources from the sample deviate from the classical $R_{H\beta} - L_{5100}$ relation ([Grier et al. 2017; Czerny et al. 2019](#)), and our aim is to find properties which characterize their departure from the scaling law in the best way. [Du et al. \(2016\)](#) suggested that accretion rate is the key parameter, so we calculate the related parameters uniformly for our sample.

In order to have an agreement in the computations of AGN parameters, we recompute the values following the same methods and using the same constant factors. The black hole mass (M_{BH}) is estimated following the well-known relation:

$$M_{BH} = f_{BLR} \frac{R_{BLR} v^2}{G} \quad (1)$$

where G is the gravitational constant, f_{BLR} is the virial factor, R_{BLR} is the broad line region size, and v is the velocity field in the BLR which is typically represented by the full-width at half maximum (FWHM) of the emission line. The virial factor takes into account geometry, kinematics, and inclination angle of the BLR. Its value is frequently adopted as $f_{BLR} \sim 1$ for single-epoch estimations ([Woo et al. 2015](#)). However, it can introduce an error in the M_{BH} determination by a factor of 2–3. Recently [Mejía-Restrepo et al. \(2018\)](#) proposed that the virial factor is anti-correlated with the FWHM of broad emission line. For the H β line the relation is given by,

$$f_{BLR}^c = \left(\frac{FWHM_{obs}}{4550} \right)^{-1.17}, \quad (2)$$

with $FWHM_{obs}$ in units of km s $^{-1}$. This representation could indicate a disk-like geometry for the BLR and/or cloud motions or winds induced by the radiation force.

The best method to estimate the virial factor is through the relation $M_{BH} - \sigma^*$ where the stellar absorption features can be observed ([Woo et al. 2013](#)), however it is not always possible. In order to explore the effects of a different virial factor expression over the black hole mass and accretion parameters (Eddington ratio and dimensionless accretion rate), we have computed the M_{BH} using $f_{BLR} = 1$ and $f_{BLR}^c \propto FWHM^{-1.17}$ (See Section 3.3). In Table 2, we report mass M_{BH} considering $f_{BLR} = 1$. In order to estimate the accretion rate, we use the dimensionless accretion rate introduced by [Du et al. \(2016\)](#):

$$\dot{M} = 20.1 \left(\frac{l_{44}}{\cos i} \right)^{3/2} m_7^{-2}, \quad (3)$$

where l_{44} is the luminosity at 5100 Å in units of 10^{44} erg s $^{-1}$, i is inclination angle of disk to the line of sight, and m_7 is the black hole mass in units of $10^7 M_{\odot}$. We considered $\cos i = 0.75$, which is the mean disk inclination for type 1 AGN. It is estimated considering a torus axis co-aligned with the disk axis and a torus covering factor of 0.5 [Du et al. \(2016\)](#). Sources with $\dot{M} \gtrsim 3$ are highly accreting AGN and host a

slim accretion disk (Wang et al. 2014b). \dot{M} with $f_{\text{BLR}}=1$ is reported in the column 3 of Table 2. SEAMBH sample has on average the largest dimensionless accretion rate, $\dot{M} \sim 139.5$, which is expected due to the selection criteria of the sample. SDSS-RM sample has the mean $\dot{M} \sim 11.9$, where one-third of the sources are classified as high accretors. The Bentz collection has the smallest mean value of ~ 7.9 . As for the two remaining objects, 3C273 is classified as a high accretor ($\dot{M} \sim 51.7$) and NGC5548 is one the source with lowest accretors in the sample, $\dot{M} \sim 0.01$.

We also consider the Eddington ratio, $L_{\text{bol}}/L_{\text{Edd}}$, as an estimation of the accretion rate, where L_{bol} is the bolometric luminosity and L_{Edd} is the Eddington luminosity defined by $L_{\text{Edd}} = 1.5 \times 10^{38} \left(\frac{M_{\text{BH}}}{M_{\odot}} \right)$. In order to determine L_{bol} , we use the bolometric correction factor at 5100Å proposed by Richards et al. (2006), $\text{BC}_{5100} = 10.33$. Although $L_{\text{bol}}/L_{\text{Edd}}$ depends upon the bolometric correction factor used, it has given good results in the identification of high accretion sources, which show $L_{\text{bol}}/L_{\text{Edd}} > 0.2$ (Sulentic et al. 2017). The limit considered for \dot{M} and $L_{\text{bol}}/L_{\text{Edd}}$ in order to identify highly accreting sources is analogous, since both parameters are well correlated Capellupo et al. (e.g. 2016). Average $L_{\text{bol}}/L_{\text{Edd}}$ values are as follows: 1.6, 0.3 and 0.2 for SEAMBH, SDSS-RM and Bentz collection respectively. $L_{\text{bol}}/L_{\text{Edd}}$ with a virial factor equal to 1 is shown in the fourth column of Table 2.

2.4. Virial factor effect on black hole mass and accretion parameters

Dimensionless accretion rate and Eddington ratio depend on the black hole mass, thus they are affected by the virial factor. Considering the virial factor anti-correlated with the FWHM of H β (f_{BLR}^c), dimensionless accretion rate and Eddington ratio change by a factor $(f_{\text{BLR}}^c)^{-2}$ and $(f_{\text{BLR}}^c)^{-1}$ respectively, i.e.,

$$\begin{aligned} \dot{M}^c &= (f_{\text{BLR}}^c)^{-2} \dot{M}, \\ \frac{L_{\text{bol}}}{L_{\text{Edd}}^c} &= (f_{\text{BLR}}^c)^{-1} \left(\frac{L_{\text{bol}}}{L_{\text{Edd}}} \right). \end{aligned} \quad (4)$$

Therefore, new values for the accretion parameters can be estimated from the ones reported in Table 2. The virial factor selection changes considerably the accretion parameters and the dispersion associated with other physical parameters (see section 3.3).

2.5. Variability characteristics

In order to have an estimation of the variability amplitude, we will consider the parameter F_{var} (Rodríguez-Pascual et al. 1997). It estimates the rms of the intrinsic variability relative to the mean flux,

$$F_{\text{var}} = \frac{(\sigma^2 - \Delta^2)^{1/2}}{\langle f \rangle}, \quad (5)$$

where σ^2 is the variance of the flux, Δ is the mean square value of the uncertainties (Δ_i) associated with each flux measurement (f_i), and $\langle f \rangle$ is the mean flux. Their definitions are as follows,

$$\begin{aligned} \sigma^2 &= \frac{1}{1-N} \sum_{i=1}^N (f_i - \langle f \rangle)^2, \\ \Delta^2 &= \frac{1}{N} \sum_{i=1}^N \Delta_i^2, \\ \langle f \rangle &= \frac{1}{N} \sum_{i=1}^N f_i. \end{aligned} \quad (6)$$

F_{var} parameter has been reported for all the objects of Bentz collection (Peterson et al. 2004; Bentz et al. 2009; Denney et al. 2010; Bentz et al. 2014; Barth et al. 2013; Pei et al. 2014; Bentz et al. 2016a,b; Fausnaugh et al. 2017) and some SEAMBH objects (Hu et al. 2015). For the remaining SEAMBH sources, we estimate F_{var} from the light curves available in the literature (Du et al. 2015, 2016, 2018) following the Equations (5) and (6). In the case of the SDSS-RM sample, we use the *fractional RMS variability* provided by Shen et al. (2018) (see their Table 2). Using the luminosities reported in Table 1, we can convert this quantity to F_{var} . The object J142103 shows $\sigma^2 - \Delta^2 < 0$, indicating that it does not present a significant variability, such as the one that has been reported in other objects (e.g. Sánchez et al. 2017). F_{var} values are reported in the last column of Table 2.

3. ACCRETION RATE DEPENDENCE ALONG THE $R_{\text{H}\beta} - L_{5100}$ RELATION

3.1. $R_{\text{H}\beta} - L_{5100}$ relation

With the information reported in Table 1, we are able to build the $R_{\text{H}\beta} - L_{5100}$ relation,

$$\begin{aligned} \log \left(\frac{R_{\text{BLR}}}{1\text{lt-day}} \right) &= (1.527 \pm 0.31) + \\ &0.533_{-0.033}^{+0.035} \log \left(\frac{L_{5100}}{10^{44} L_{\odot}} \right). \end{aligned} \quad (7)$$

We explored if FWHM and the equivalent width show a similar trend along the $R_{\text{H}\beta} - L_{5100}$ relation, but we can not find any clear pattern.

3.2. Testing cadence in SDSS-RM sample

The monitoring performed for the SDSS-RM sample is relatively short (only 180 days) taking into account that their sources are at relatively large redshift and some of them are rather bright. Expected delay could be close to the duration of the campaign. In addition, the number of spectroscopic measurements is not very high (only 32). This may

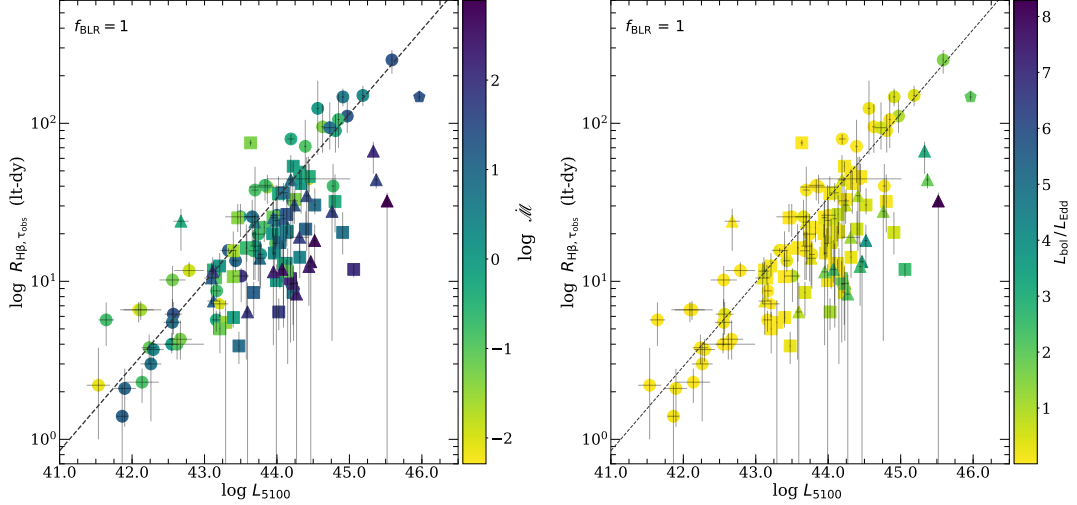


Figure 1. $R_{H\beta} - L_{5100}$ relation for SEAMBH (triangles), SDSS-RM (squares), Bentz Collection (circles), NGC5548 and 3C273 (pentagons). Colors indicate the variation in dimensionless accretion rate (\dot{M} , left) and Eddington ratio ($L_{\text{bol}}/L_{\text{Edd}}$, right). Dashed black line corresponds to the expected $R_{H\beta} - L_{5100}$ relation from Bentz et al. (2013). The dimensionless accretion parameter and the Eddington ratio have been computed considering $f_{\text{BLR}}=1$.

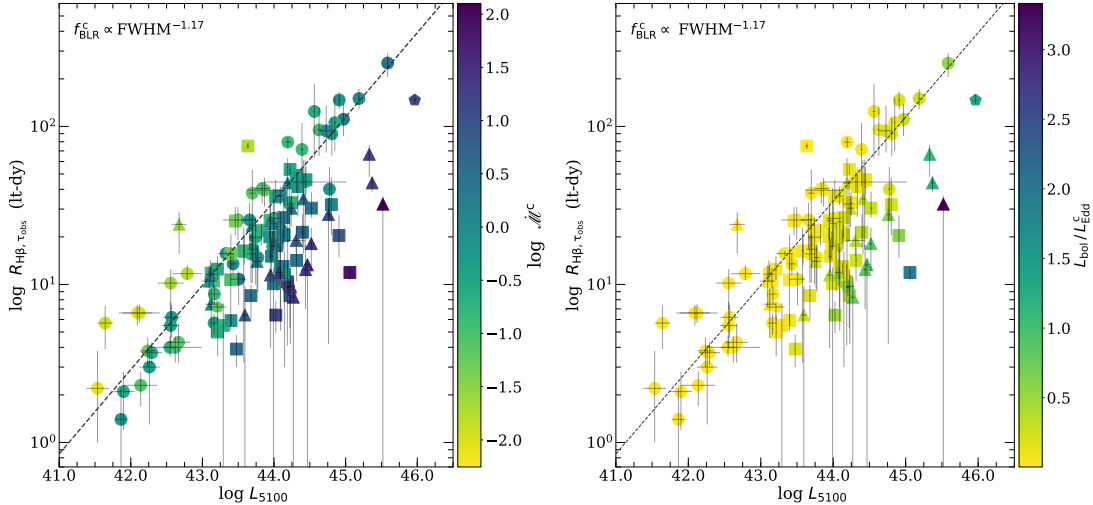


Figure 2. The same figure as in Figure 1, but considering the virial factor dependence $f_{\text{BLR}}^c \propto \text{FWHM}^{-1.17}$.

cast some doubts whether the estimated time delays are measured reliably. Thus we performed simulations of the expected time delays assuming that the sources follow the standard $R_{H\beta} - L_{5100}$ relation and using the observational cadence. The results are presented in the Appendix A and they show that both the duration of the observation and the cadence should not strongly affect the measured delays.

3.3. Correction for the time delay

SEAMBH team have done an important progress in understanding the reverberation mapping in highly accreting sources (Wang et al. 2014c; Du et al. 2014; Hu et al. 2015;

Du et al. 2015, 2016, 2018). They found that AGN with $\dot{M} \gtrsim 3$ have time delay (τ_{obs}) shorter than expected from the $R_{H\beta} - L_{5100}$ scaling law (Bentz et al. 2013). The deviation can be estimated by the parameter,

$$\Delta R_{H\beta} = \log \left(\frac{R_{H\beta}}{R_{H\beta_{R-L}}} \right) = \log \left(\frac{\tau_{\text{obs}}}{\tau_{H\beta_{R-L}}} \right), \quad (8)$$

where $\tau_{H\beta_{R-L}}$ is the time delay corresponding to the ones expected from the $R_{H\beta} - L_{5100}$ relation, see Equation (7). Figure 3 and 4 show $\Delta R_{H\beta}$ as a function of \dot{M} and $L_{\text{bol}}/L_{\text{Edd}}$ considering f_{BLR} and f_{BLR}^c . In all four cases, the largest $\Delta R_{H\beta}$ are associated with the highest \dot{M} and

$L_{\text{bol}}/L_{\text{Edd}}$, the difference is in the scattering along the relations. We perform a orthogonal linear fit in order to get the linear trend, and estimate the Pearson coefficient (P) and the root-mean-squared error (rms) to measure the correlation and dispersion along the trend line. The linear relations, Pearson coefficient and rms values are as follows,

$$f_{\text{BLR}} \left\{ \begin{array}{l} \Delta R_{\text{H}\beta, \dot{\mathcal{M}}} = (-0.143 \pm 0.018) \log \dot{\mathcal{M}} + (-0.136 \pm 0.023) \\ P = 0.572, \quad rms = 0.243 \\ \\ \Delta R_{\text{H}\beta, L_{\text{Edd}}} = (-0.271 \pm 0.030) \log \frac{L_{\text{bol}}}{L_{\text{Edd}}} + (-0.396 \pm 0.032) \\ P = 0.605, \quad rms = 0.626 \end{array} \right. \quad (9)$$

$$f_{\text{BLR}}^c \left\{ \begin{array}{l} \Delta R_{\text{H}\beta, \dot{\mathcal{M}}^c} = (-0.283 \pm 0.017) \log \dot{\mathcal{M}}^c + (-0.228 \pm 0.016) \\ P = 0.822, \quad rms = 0.172 \\ \\ \Delta R_{\text{H}\beta, L_{\text{Edd}}^c} = (-0.394 \pm 0.030) \log \frac{L_{\text{bol}}}{L_{\text{Edd}}^c} + (-0.589 \pm 0.036) \\ P = 0.744, \quad rms = 0.199 \end{array} \right. \quad (10)$$

The information given by the Pearson coefficients and rms values indicates that relations between $\Delta R_{\text{H}\beta}$ and accretion parameters are stronger when the virial factor anti-correlated with the FWHM is used, see Equation (10). We are able to propose a correction for the time delay based on the accretion parameters which recovers the value expected from the $R_{\text{H}\beta} - L_{5100}$ relation. Since P and rms favor $\dot{\mathcal{M}}^c$, the correction used will be based on it and not on $L_{\text{bol}}/L_{\text{Edd}}^c$. The scattering in Eddington ratio could be higher due to the large uncertainties associated with the bolometric correction.

Time delay corrected for the effect of the dimensionless accretion rate can be estimated by the relation,

$$\tau_{\text{corr}}(\dot{\mathcal{M}}^c) = 10^{-\Delta R_{\text{H}\beta}(\dot{\mathcal{M}}^c)} \cdot \tau_{\text{obs}}. \quad (11)$$

The quantities $\dot{\mathcal{M}}^c$, $\Delta R_{\text{H}\beta}(\dot{\mathcal{M}}^c)$ and $\tau_{\text{corr}}(\dot{\mathcal{M}}^c)$ are listed in Table 3. The $R_{\text{H}\beta} - L_{5100}$ relation with the correction for the dimensionless accretion rate is shown in the Figure 5. If we compare this new diagram with the one shown in the left panel of Figure 2, it is clear that the scattering decreases significantly along the $R_{\text{H}\beta} - L_{5100}$ relation, $\sigma_{\text{obs}} = 0.684$ vs. $\sigma_{\text{corr}} = 0.396$ in log space. With this correction, we are

able to build a better luminosity distance-redshift relation or Hubble diagram and compare them with the standard cosmological models (see section 4).

3.4. Is there break in $\dot{\mathcal{M}}=3$ for the $\Delta R_{\text{H}\beta}$ behavior?

As we show in the previous section, the relation between $\Delta R_{\text{H}\beta}$ and the dimensionless accretion rate (or Eddington ratio) can be represented by a linear fit, independently of the virial factor. However, Du et al. (2015, 2018) argue that around $\dot{\mathcal{M}}=3$ there is a break in the behavior of $\Delta R_{\text{H}\beta}$, where highly accreting sources would be characterized by optically thick and geometrically slim accretion (Wang et al. 2014b). Considering the deviation of the $R_{\text{H}\beta} - L_{5100}$ relation, sources with $\dot{\mathcal{M}} < 3$ would be associated with a $\Delta R_{\text{H}\beta} \sim 0$, while sources with $\dot{\mathcal{M}} > 3$ would show a $\Delta R_{\text{H}\beta}$, with a decreasing trend as a function of $\dot{\mathcal{M}}$. This interpretation should correspond to the relation $\Delta R_{\text{H}\beta} - \dot{\mathcal{M}}$ assuming $f_{\text{BLR}}=1$ (left panel of Figure 3), which was analyzed by Du et al. (2015, 2018). However, even in this case, there is a significant difference with our analysis which comes from the location of the SDSS-RM sample in the diagram. Du et al. (2018) include this sample in their analysis, but they use the M_{BH} estimated from Grier et al. (2017), who adopt a $f_{\text{BLR}}=4.47$ adequate for a M_{BH} estimation based on $\sigma_{\text{line,rms}}$ (Woo et al. 2015). In our estimation, some SDSS-RM objects are located around $\dot{\mathcal{M}}=3$, covering the empty region shown in their Figure 3. In order to get a possible difference between the sources with $\dot{\mathcal{M}} < 3$ and > 3 , we perform a two-sample Kolmogorov-Smirnov (K-S) test. We find a value of 0.344 with a probability of $p_{\text{KS}} \sim 0.003$. A similar p_{KS} is reported by Du et al. (2015), that according to them is enough to demonstrate that $\Delta R_{\text{H}\beta} \sim 0$ for $\dot{\mathcal{M}} < 3$. If we apply the K-S test for $\Delta R_{\text{H}\beta} - L_{\text{bol}}/L_{\text{Edd}}$ with $f_{\text{BLR}}=1$, we get a value 0.392 and $p_{\text{KS}} = 0.0004$, which favors the difference at $\dot{\mathcal{M}}=3$. On the other hand, if we consider a virial factor anti-correlated with the FWHM of $\text{H}\beta$, $\Delta R_{\text{H}\beta}$ decreases progressively as function of $\dot{\mathcal{M}}^c$ or $L_{\text{bol}}/L_{\text{Edd}}^c$ (Figure 4). It is confirmed by the K-S test, we get 0.771 with a $p_{\text{KS}} = 2.9 \times 10^{-11}$ and 0.663 with a $p_{\text{KS}} = 1.8 \times 10^{-9}$ for $\dot{\mathcal{M}}^c$ and $L_{\text{bol}}/L_{\text{Edd}}^c$, respectively.

In all four cases, there is a different behavior around $\dot{\mathcal{M}}=3$. For all cases, $\Delta R_{\text{H}\beta}$ median is 0.09 for $\dot{\mathcal{M}} < 3$ (or $L_{\text{bol}}/L_{\text{Edd}} < 0.2$), however the scattering is higher with a virial factor equal to 1. For the high accretion rate, $\Delta R_{\text{H}\beta}$ median is 0.26 and 0.31 for $\dot{\mathcal{M}}$ and $L_{\text{bol}}/L_{\text{Edd}}$, and 0.61 and 0.50 for $\dot{\mathcal{M}}^c$ and $L_{\text{bol}}/L_{\text{Edd}}^c$, respectively. However, from Figure 2 we see that very low accretion objects have a $\Delta R_{\text{H}\beta} > 0$ for a virial factor anti-correlated with the FWHM. As we have shown in the previous section, we can represent the relation between $\Delta R_{\text{H}\beta}$ and accretion parameters by a linear fit in the whole log space, without any break, which is supported by the Pearson coefficient and rms value. We do

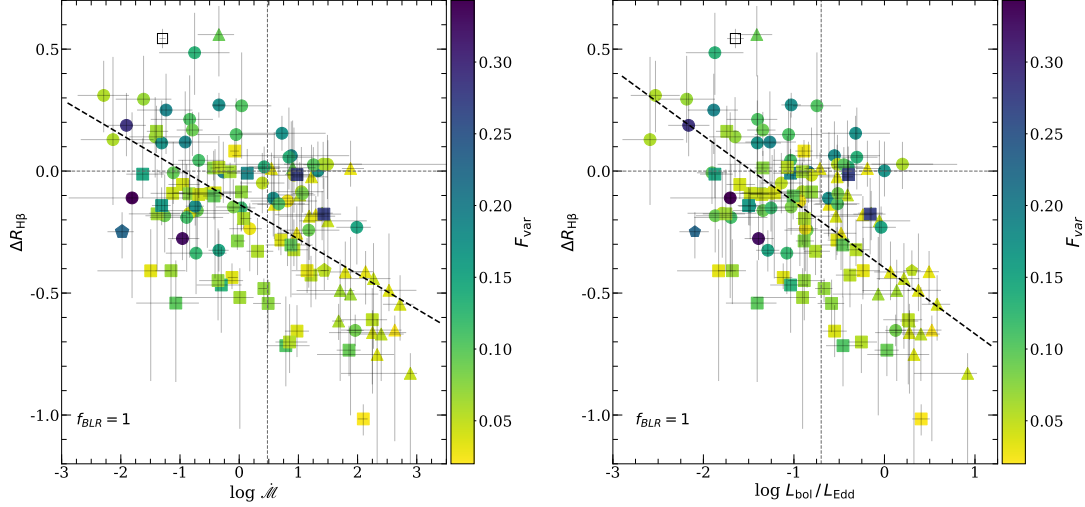


Figure 3. Relation between $\Delta R_{H\beta}$ and \dot{M} (left) and $L_{\text{bol}}/L_{\text{Edd}}$ (right) using $f_{\text{BLR}}=1$. Symbols are the same as Figure 1. Marker colors indicate the variation in F_{var} . Empty marker corresponds to the quasar J142103 (See section 2.5). In both panels dashed horizontal correspond to $\Delta R_{H\beta}=0$ and black thick line show the best orthogonal linear fit. Vertical lines corresponds to and $\dot{M}=3$ and $L_{\text{bol}}/L_{\text{Edd}}=0.2$.

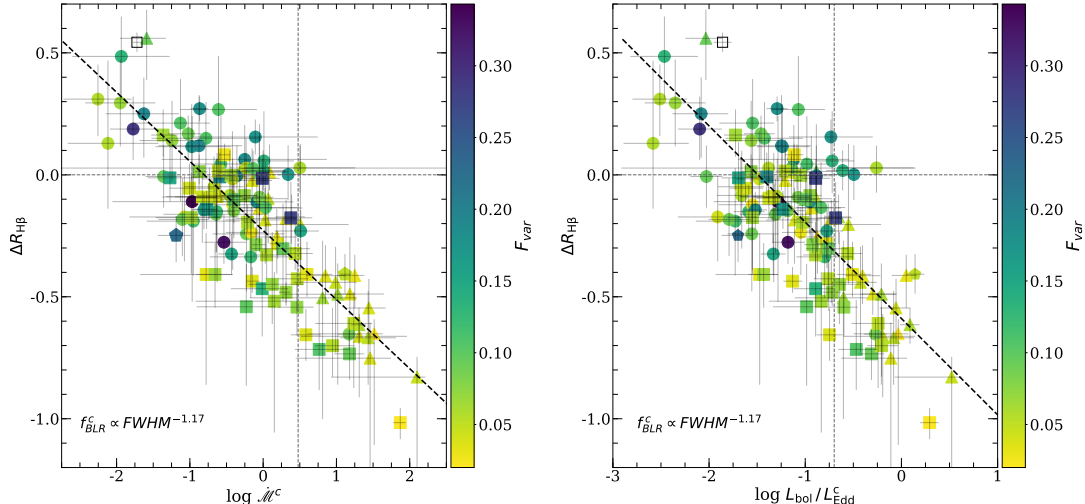


Figure 4. Relation between $\Delta R_{H\beta}$ and \dot{M}^c (left) and $L_{\text{bol}}/L_{\text{Edd}}^c$ (right) using $f_{\text{BLR}}^c \propto \text{FWHM}^{-1.17}$. Description of markers, colors and lines are the same in Figure 3.

not see any evidence of a break around $\dot{M}=3$, specially in the cases with a virial factor anti-correlated with the FWHM of $H\beta$.

The virial factor is one of the most important uncertainties in the black hole mass determination and accretion parameters. According to Mejía-Restrepo et al. (2018), the virial factor f_{BLR}^c includes the correction for the orientation effect, then \dot{M}^c would show an accurate estimation which is reflected in the scattering of the measurement, particularly when it is compared with the other parameters. However, their results are based on Shakura–Sunyaev (SS) disk (Shakura & Sunyaev 1973), which is appropriated for their

sample, where $\sim 90\%$ of the objects show a low accretion rate and they can be perfectly presented by a SS model disk (Capellupo et al. 2016). Our sample includes 20–50% of high accretors, depending on the virial factor considered. According to Wang et al. (2014b), in high accretors the slim disk produces an anisotropic radiation field, which divides the BLR into two regions with distinct incident ionizing photon fluxes. Using the code BRAINS, Li et al. (2018) demonstrated that two region model is better than a simple one for Mrk 142, a typical high accretor source. Therefore, the incident radiation flux and geometry are more complex in highly accreting AGN. New spectral energy distributions (SED) models for

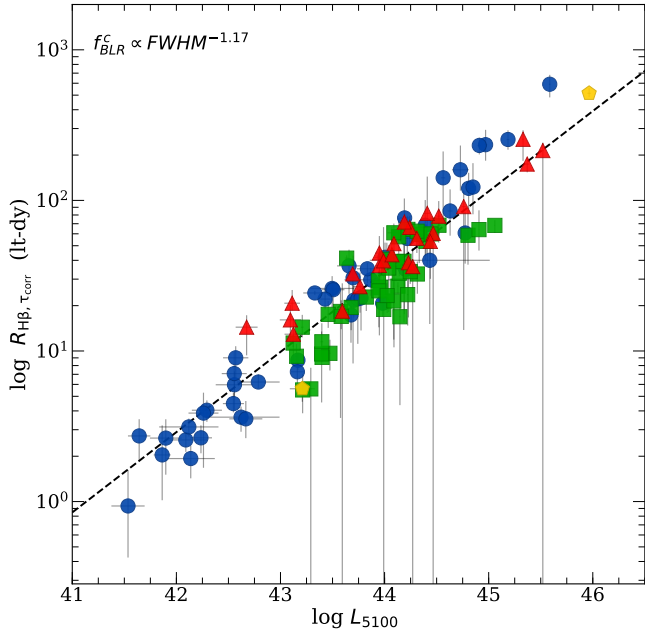


Figure 5. $R_{H\beta} - L_{5100}$ relation with time delay corrected by dimensionless accretion rate effect. Red triangles correspond to the SEAMBH sample, green squares correspond to the SSDS-RM sample, blue circles correspond to Bentz collection, and yellow pentagons mark the position of NGC 5548 and 3C 273. Dashed black line corresponds to the expected $R_{H\beta} - L_{5100}$ relation from Bentz et al. (2013).

slim disk are required, in order to get a better estimation in the virial factor for this kind of objects.

3.5. Relation between F_{var} and accretion parameters

Studies of large quasar samples showed that amplitude of the variability is anti-correlated with Eddington ratio (Wilhite et al. 2008; MacLeod et al. 2010; Simm et al. 2016; Rakshit & Stalin 2017; Sánchez-Sáez et al. 2018; Li et al. 2018). F_{var} measures the excess of variability above the noise level and it can be used as an estimator of this effect. As we showed in the previous section, $\Delta R_{H\beta}$ is anti-correlated with the dimensionless accretion rate and Eddington ratio. In Figure 3 and 4 we show the change of F_{var} along the relation $\Delta R_{H\beta} - \dot{M}$ and $\Delta R_{H\beta} - L_{\text{bol}}/L_{\text{Edd}}$ using different virial factors. In all the cases, the minimum F_{var} values tend to be associated with the highest \dot{M} (and $L_{\text{bol}}/L_{\text{Edd}}$) and the smallest $\Delta R_{H\beta}$ values.

Sánchez-Sáez et al. (2018) report that the amplitude of variability A is strongly related with σ_{rms} (Sánchez et al. 2017), which is the square of F_{var} . Estimating σ_{rms} , we compute the Spearman coefficient (ρ_s) in order to confirm the relation between the accretion parameters and variability. The stronger relation is given by \dot{M} and \dot{M}^c , with a $\rho_s = -0.397$ ($p = 7.9 \times 10^{-6}$) and $\rho_s = -0.374$

($p = 1.6 \times 10^{-5}$), respectively. Spearman coefficients for $L_{\text{bol}}/L_{\text{Edd}}$ and $L_{\text{bol}}/L_{\text{Edd}}^c$ are -0.341 ($p = 1.8 \times 10^{-4}$) and -0.259 ($p = 1.8 \times 10^{-3}$), respectively. Sánchez-Sáez et al. (2018) report a Spearman coefficient for $L_{\text{bol}}/L_{\text{Edd}}$ of $\rho_s = -0.22$ ($p = 1 \times 10^{-8}$), which is comparable to the value found by us. Dimensionless accretion rate seems to be more strongly related with the other physical parameters (e.g. F_{var} and $\Delta R_{H\beta}$) than the Eddington ratio, which is probably linked with the bolometric luminosity uncertainties.

According to Allevato et al. (2013), F_{var} is strongly affected by biases, for example in the structure of variability or length of the light curve, therefore it has to be treated with caution. In our sample, some of the SDSS-RM object were observed in the red-edge of the spectrum, where the telluric lines are difficult to remove, and considering the short cadence of the light curve, it could also affect the relation. However, under the proper observational conditions, F_{var} could be another of the possible variability parameters, giving information about the physical properties of the AGN. Surveys such as the Large Synoptic Survey Telescope will be able to estimate this parameter for a large quasar sample, and following the relations like those presented in this work, this can provide information about the accretion disk structure, accretion process and the size of the BLR. A multivariate analysis is needed to get a correct relation between the F_{var} (or σ_{rms}) and the dimensionless accretion rate, which is out of the scope of this work.

4. HUBBLE DIAGRAM

We now perform a simple test of the prospects for quasar application for cosmology by locating the sources on the Hubble diagram. Now we only use their measured time delay (τ_{obs} and τ_{corr}) and the observed flux at 5100 Å rest-frame (F_{5100}). We use Equation (7) to determine L_{5100} , and finally to measure the luminosity distance, D_{L} ,

$$D_{\text{L}} = \left(\frac{L_{5100}}{4\pi F_{5100}} \right)^{1/2}. \quad (12)$$

Left panel of Figure 6 shows the luminosity distance estimated with τ_{obs} , which exhibits large scattering. We now take all objects from our sample plotted in Figure 5 and assume they follow precisely the $R_{H\beta} - L_{5100}$ relation while we relax the assumption that their absolute luminosity L_{5100} is known. Repeating the same exercise, we find that the scatter is strongly reduced (see right panel of Figure 5). This is better shown in the corresponding bottom panels where we plot the residuals between the logarithm of the expected ($D_{\text{L,mod}}$) and estimated luminosity distance (D_{L}). It is clear that the dispersion decreases after the correction, which is supported by the rms value (0.287 vs. 0.182). Here plotted uncertainties come only from the uncertainty in the time delay measurement. As a guide, in both panels we plot

the standard Λ CDM model with the parameters (Planck Collaboration 2013): $H_0 = 67 \text{ km s}^{-1} \text{ Mpc}^{-1}$, $\Omega_\Lambda = 0.68$, $\Omega_m = 0.32$ (continuous black line Figure 6). We see that while in the left panel a significant fraction of points implied too small distances, after the accretion-rate dependent correction the points are distributed close to the line.

To demonstrate this quantitatively, in Figure 7 we give the distribution of the $\log \frac{D_{L,\text{mod}}}{D_L}$. The distribution before the correction shows clear asymmetry to the right, and it is centered at 0.123. After applying the correction, the distribution is centered at 0.055. The standard deviation also shows an improvement (0.19 vs. 0.31). With this information we can think of constraining the cosmological parameters.

In order to illustrate better the accuracy of determination of the cosmological parameters, we performed formal computations of the best cosmological model. We assumed a standard Λ CDM model, and the value of the Hubble constant $67 \text{ km s}^{-1} \text{ Mpc}^{-1}$, used in the computations of corrections related to the accretion rate (see Section 3.3). We did not modify the parameters in Equation (7) relating the time delay and the absolute luminosity. Then we searched for the minimum of the function

$$\chi^2 = \sum_{i=1}^N \frac{(\log(D_{L,\text{mod}}^i) - \log(D_{L,\text{obs}}^i))^2}{(\log(1 + b_i)^2 + \sigma^2)}, \quad (13)$$

where N is the total number of sources in the sample, and b_i is the relative error in the luminosity distance determination implied by uncertainty in the measured time delay. We introduced a quantity σ following the approach by Risaliti & Lusso (2015). This quantity describes the dispersion in the sample, which is larger than the claimed measurement errors. The result is shown in Figure 8, left panel. The best fit is in edge of the domain (minimum χ^2), however it is consistent with the standard cosmology, and the accepted parameter values are consistent with our results within 2σ . The errors are still large, due to the limited number of objects (117 in the full sample), and possibly also to heterogenic way of data reduction—time delays were measured by various authors, using different methods. We checked if we can improve the constraints by using only higher-redshift sources $z > 0.4$ (30 sources), but this caused the large shift of the best fit (from $\Omega_m = 1.0, \Omega_\Lambda = 1.34$ to $\Omega_m = 0.4, \Omega_\Lambda = 0.1$) and the errors contour were then even larger due to the reduced number of objects.

The effective use of the method requires an increase of the number of reverberation-measured objects by a factor of at least 5. There are some prospects for new time delay measurements, particularly at larger redshifts. First, the SDSS-RM campaign continues. Second, the project of monitoring 500 quasars with Oz-DES survey (King et al. 2015) is likely to finish soon. Thus, the method itself looks quite promising.

5. CONCLUSIONS

In this work, we confirmed that the time delay measured during the reverberation mapping campaigns is affected by the accretion rate of individual sources. Considering the deviation from the $R_{H\beta} - L_{5100}$ relation and the corresponding accretion rate, we propose the correction based on $\Delta R_{H\beta}$, which is a power-law function of the dimensionless accretion rate parameter. This correction recovers the expected time delay, decreasing the scattering and providing a proper estimate of the BLR size. Using the corrected values, we built the Hubble diagram, obtaining consistent results with the Λ CDM model within 2σ confidence level. However, uncertainties are still large, which could be mitigated by significantly increasing the number of sources, especially towards larger redshifts.

We used the dimensionless accretion rate and the Eddington ratio to estimate the effect of the accretion rate. The former one appears to show a better correlation with other physical quantities, which could be related by large uncertainties associate to the bolometric luminosity. We also explore the use of a virial factor anti-correlated with the FWHM of $H\beta$ line. The black hole mass and the accretion parameters give a lower dispersion in the comparison with the case $f_{\text{BLR}}=1$. Since the virial factor anti-correlated with the FWHM includes the correction for the source orientation (Mejía-Restrepo et al. 2018), it can explained the lower scattering. However, a more detailed analysis is required to confirm the use of this virial factor, specially for the highly accreting objects.

In addition, we also confirm the anti-correlation between the variability and the accretion parameters, using the parameter F_{var} . Although F_{var} is sensible to the monitoring conditions and the quality of observations, it shows the same behavior as similar parameters, such as the variability amplitude. Large surveys such as LSST will observe this kind of properties and it is important to establish the relation with other physical parameters. This result supports that the accretion parameter (the Eddington ratio or the dimensionless accretion rate) is the main driver of many of the quasar properties (Marziani et al. 2001; Shen & Ho 2014) such as variability or outflows. It could be linked to a different type of the accretion disk structure (Wang et al. 2014b).

ACKNOWLEDGEMENTS

The project was partially supported by National Science Centre, Poland, grant No. 2017/26/A/ST9/00756 (Maestro 9), and by the MNiSW grant DIR/WK/2018/12. VK acknowledges Czech Science Foundation No. 17-16287S. We acknowledge P. Du, Y.-R. Li and J.-M. Wang for the provided data and comments that improved the paper. We acknowledge M. Bentz, C. J. Grier, J. Kuraszkiewicz, A. del

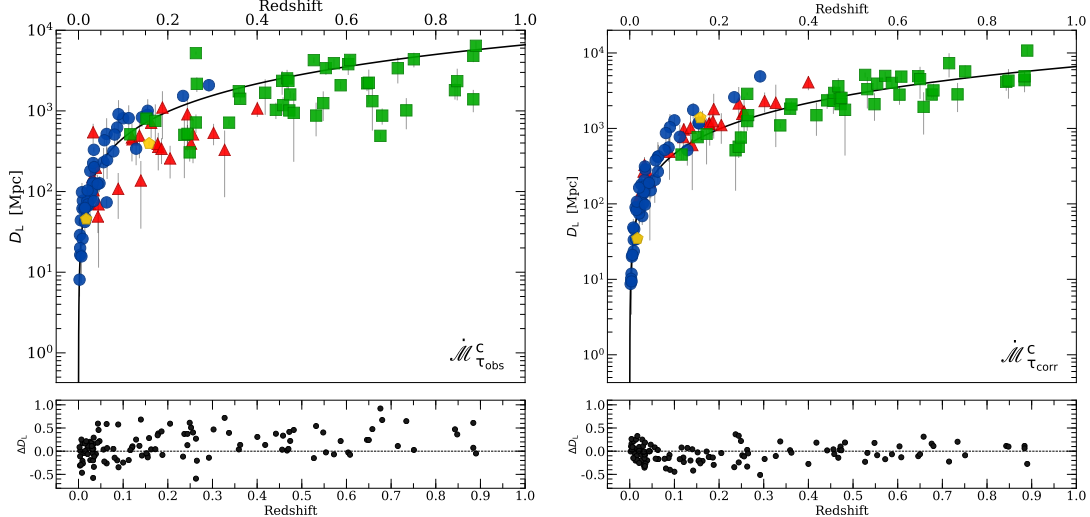


Figure 6. Hubble diagram before (left) and after (right) the correction by dimensionless accretion rate. Markers and colors are the same as in Figure 5. The black lines indicates the expected luminosity distance based on the standard Λ CDM model. In both cases, the bottom panel shows the difference between the expected luminosity distance and the observed one.

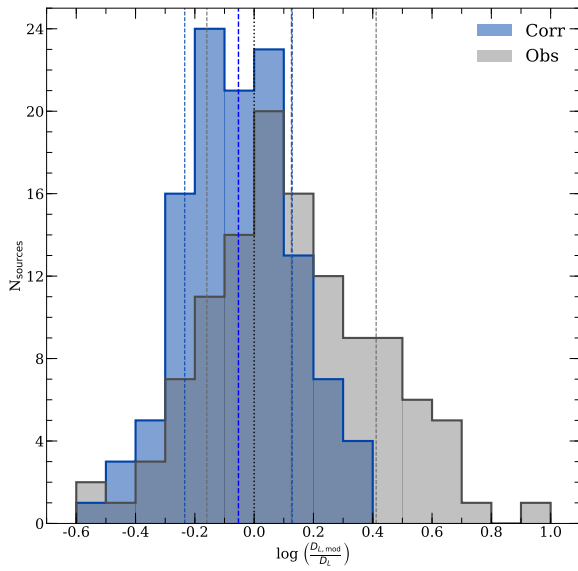


Figure 7. Distribution of the difference between the logarithm of the expected luminosity distance ($\log \frac{D_{L,mod}}{D_L}$) respect to the obtained from the observations before (gray) and after correction (blue). Vertical dashed gray and blue lines correspond to the average (thick), and $\pm 1\sigma$ values (thin) before and after correction, respectively. Vertical dotted black line marks $\log \frac{D_{L,mod}}{D_L} = 0$.

Olmo, M. Fausnaugh, J. Mejía–Restrepo and Y. Shen for the extra information required for the development of this work.

APPENDIX

A. MONTE CARLO SIMULATIONS OF THE SDSS-RM SETUP

Monitoring presented in Grier et al. (2017) is relatively short taking into account rather high redshifts and luminosities of the sources. Therefore, we performed Monte Carlo simulations with the aim to check independently whether the observational setup forces the measured time delays to be shorter than otherwise expected for a given source redshift and luminosity.

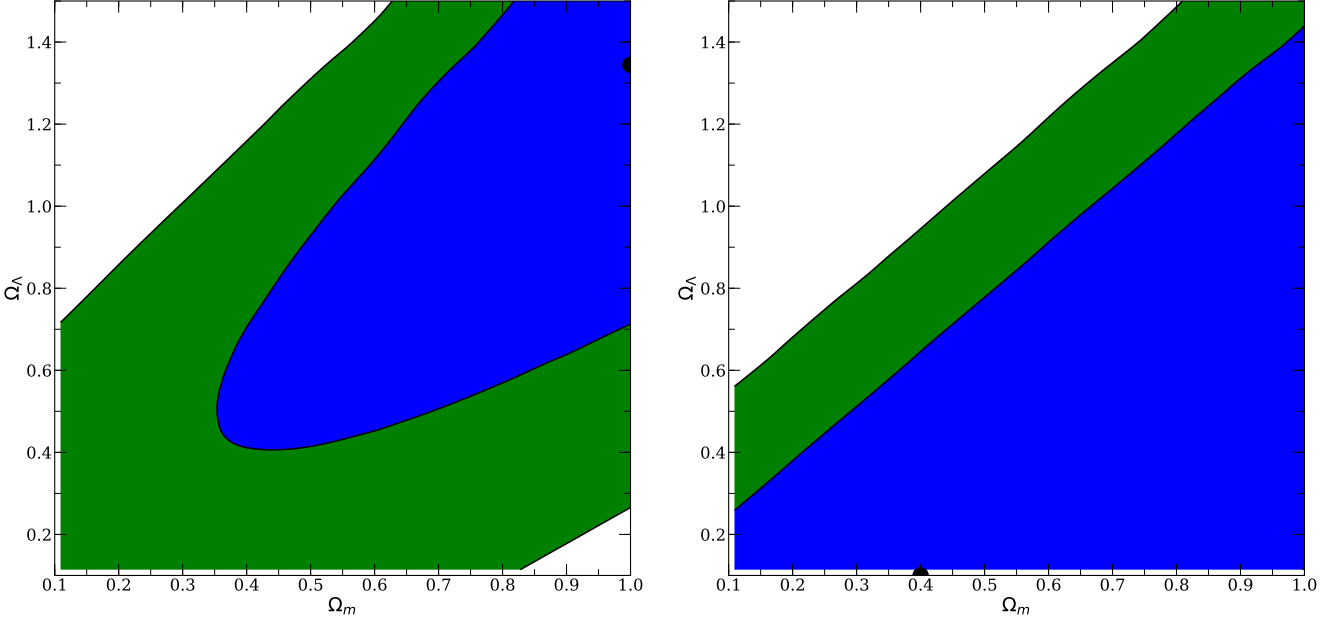


Figure 8. χ^2 behavior in the $\Omega_m - \Omega_\Lambda$ space for the full sample (left panel) and for the selected sources with only $z > 0.4$ (right panel). In both panels blue and green contours correspond to 1σ and 2σ confidence levels, respectively. Black dot marks the minimum χ^2 value, in both cases at the edge of the domain.

For this purpose, we simulated each source independently, taking into account its monochromatic luminosity, L_{5100} , and its redshift. For each source we first created 100 artificial dense light curves using Timmer & Koenig (1995) algorithm. We model the overall power density spectrum (PDS) shape assuming a power law shape with two breaks and three slopes. The high frequency slope was taken as 2.5 following Kepler results for quasars from Mushotzky et al. (2011). The high frequency break was set at 200 days for all sources, as a mean value taken from Simm et al. (2016). The slope of the middle part of PDS was taken as $s_1 = 1.2$ (Czerny et al. 1999; Simm et al. 2016). The low frequency break was fixed somewhat arbitrarily at the value ten times lower than the high frequency break, and the law frequency slope was assumed to be zero. We then exponentiated the resulting light curve, following Uttley et al. (2005), since this reproduces the log-normal distribution characteristic for the light curves of accreting sources.

The light curve describing the emission line was generated from the dense light curve above describing the continuum by shifting it by the delay expected from Equation (7) and smearing it with a Gaussian of the width equal to 0.1 of the expected time delay. Next a continuum and line light curve were created out of the dense light curve adopting the cadence in the SDSS-RM monitoring (32 observations, separated as indicated by Figure 2 in Grier et al. (2017), and sent to us by the authors. After correcting the cadence for the redshift of a given source we perform simulations in the rest frame of each source. For each of the 100 random realizations of the process we now calculate the time delay using the Interpolated Cross Correlation Function (ICCF). Finally, from these 100 realizations we calculate the mean time delay and the dispersion. In Fig. 9 we compare the time delay from our Monte Carlo simulations with the time delay expected from Equation (7) and used in the simulations. We see that the dispersion in the time delay obtained from simulations is in general higher than the errors quoted by Grier et al. (2017). We see some trend to obtain somewhat shorter time delay than assumed, due to the specific cadence used in the observations. However, for the majority of the sources the implied underestimation of the BLR radius $\Delta R_{H\beta}$ is below 0.1, much smaller than the actual departure from the standard $R_{H\beta} - L_{5100}$ law, and well within the error. Only one source, J141856, is strongly affected by the cadence of the SDSS-RM, and its measured delay is likely much higher than 15.8 days reported by Grier et al. (2017). This source was not considered in the presented analysis, due to the low quality of its spectra, where the $H\beta$ profile is completely destroyed. In our simulations, assuming a delay of 203 days in the quasar rest-frame, we obtained the probability of 0.32 to obtain the delay within the upper limit of the delay measured for this source (21.8 days), and a probability of 0.29 to get a delay shorter than the measured value of 15.8 days.

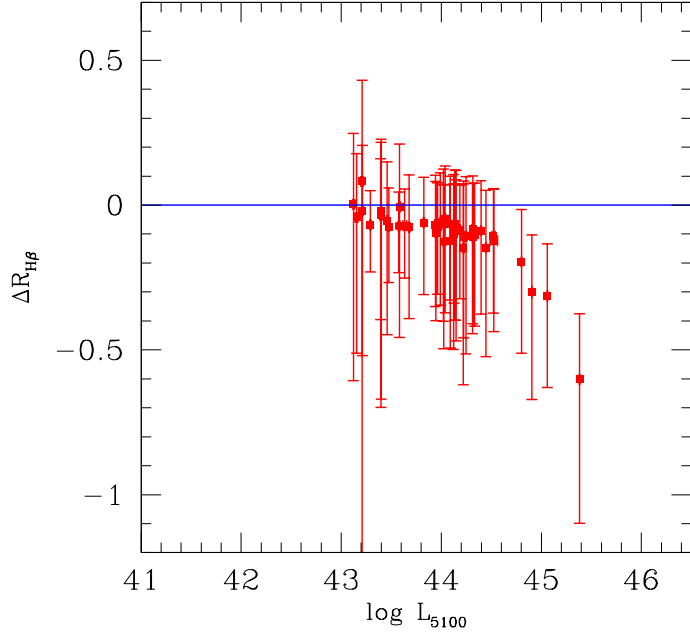


Figure 9. The estimate of the systematic offset in the measured time delay in the sub-sample of Grier et al. (2017) due to the cadence. In the case of four brightest objects the measured delay is underestimated, but the effect seems very strong only in the case of one object, J141856.

REFERENCES

Allevato, V., Paolillo, M., Papadakis, I., & Pinto, C. 2013, ApJ, 771, 9, doi: [10.1088/0004-637X/771/1/9](https://doi.org/10.1088/0004-637X/771/1/9)

Barth, A. J., Pancoast, A., Bennert, V. N., et al. 2013, ApJ, 769, 128, doi: [10.1088/0004-637X/769/2/128](https://doi.org/10.1088/0004-637X/769/2/128)

Bentz, M. C., Cackett, E. M., Crenshaw, D. M., et al. 2016a, ApJ, 830, 136, doi: [10.3847/0004-637X/830/2/136](https://doi.org/10.3847/0004-637X/830/2/136)

—. 2016b, ApJ, 830, 136, doi: [10.3847/0004-637X/830/2/136](https://doi.org/10.3847/0004-637X/830/2/136)

Bentz, M. C., Peterson, B. M., Netzer, H., Pogge, R. W., & Vestergaard, M. 2009, ApJ, 697, 160, doi: [10.1088/0004-637X/697/1/160](https://doi.org/10.1088/0004-637X/697/1/160)

Bentz, M. C., Denney, K. D., Grier, C. J., et al. 2013, ApJ, 767, 149, doi: [10.1088/0004-637X/767/2/149](https://doi.org/10.1088/0004-637X/767/2/149)

Bentz, M. C., Horenstein, D., Bazhaw, C., et al. 2014, ApJ, 796, 8, doi: [10.1088/0004-637X/796/1/8](https://doi.org/10.1088/0004-637X/796/1/8)

Brott, I., de Mink, S. E., Cantiello, M., et al. 2011, A&A, 530, A115, doi: [10.1051/0004-6361/201016113](https://doi.org/10.1051/0004-6361/201016113)

Capellupo, D. M., Netzer, H., Lira, P., Trakhtenbrot, B., & Mejía-Restrepo, J. 2016, MNRAS, 460, 212, doi: [10.1093/mnras/stw937](https://doi.org/10.1093/mnras/stw937)

Czerny, B., & Hrynewicz, K. 2011, A&A, 525, L8, doi: [10.1051/0004-6361/201016025](https://doi.org/10.1051/0004-6361/201016025)

Czerny, B., Hrynewicz, K., Maity, I., et al. 2013, A&A, 556, A97, doi: [10.1051/0004-6361/201220832](https://doi.org/10.1051/0004-6361/201220832)

Czerny, B., Schwarzenberg-Czerny, A., & Loska, Z. 1999, MNRAS, 303, 148, doi: [10.1046/j.1365-8711.1999.02196.x](https://doi.org/10.1046/j.1365-8711.1999.02196.x)

Czerny, B., Modzelewska, J., Petrogalli, F., et al. 2015, Advances in Space Research, 55, 1806, doi: [10.1016/j.asr.2015.01.004](https://doi.org/10.1016/j.asr.2015.01.004)

Czerny, B., Li, Y.-R., Hrynewicz, K., et al. 2017, ApJ, 846, 154, doi: [10.3847/1538-4357/aa8810](https://doi.org/10.3847/1538-4357/aa8810)

Czerny, B., Beaton, R., Bejger, M., et al. 2018, SSRv, 214, 32, doi: [10.1007/s11214-018-0466-9](https://doi.org/10.1007/s11214-018-0466-9)

Czerny, B., Wang, J.-M., Du, P., et al. 2019, ApJ, 870, 84, doi: [10.3847/1538-4357/aaf396](https://doi.org/10.3847/1538-4357/aaf396)

Denney, K. D., Peterson, B. M., Pogge, R. W., et al. 2010, ApJ, 721, 715, doi: [10.1088/0004-637X/721/1/715](https://doi.org/10.1088/0004-637X/721/1/715)

Du, P., Hu, C., Lu, K.-X., et al. 2014, ApJ, 782, 45, doi: [10.1088/0004-637X/782/1/45](https://doi.org/10.1088/0004-637X/782/1/45)

—. 2015, ApJ, 806, 22, doi: [10.1088/0004-637X/806/1/22](https://doi.org/10.1088/0004-637X/806/1/22)

Du, P., Lu, K.-X., Zhang, Z.-X., et al. 2016, ApJ, 825, 126, doi: [10.3847/0004-637X/825/2/126](https://doi.org/10.3847/0004-637X/825/2/126)

Du, P., Zhang, Z.-X., Wang, K., et al. 2018, ApJ, 856, 6, doi: [10.3847/1538-4357/aaae6b](https://doi.org/10.3847/1538-4357/aaae6b)

Ekström, S., Georgy, C., Eggenberger, P., et al. 2012, A&A, 537, A146, doi: [10.1051/0004-6361/201117751](https://doi.org/10.1051/0004-6361/201117751)

Fausnaugh, M. M., Grier, C. J., Bentz, M. C., et al. 2017, ApJ, 840, 97, doi: [10.3847/1538-4357/aa6d52](https://doi.org/10.3847/1538-4357/aa6d52)

Gravity Collaboration, Sturm, E., Dexter, J., et al. 2018, Nature, 563, 657, doi: [10.1038/s41586-018-0731-9](https://doi.org/10.1038/s41586-018-0731-9)

Grier, C. J., Trump, J. R., Shen, Y., et al. 2017, ApJ, 851, 21, doi: [10.3847/1538-4357/aa98dc](https://doi.org/10.3847/1538-4357/aa98dc)

Groves, B. A., Heckman, T. M., & Kauffmann, G. 2006, MNRAS, 371, 1559, doi: [10.1111/j.1365-2966.2006.10812.x](https://doi.org/10.1111/j.1365-2966.2006.10812.x)

Haas, M., Chini, R., Ramolla, M., et al. 2011, A&A, 535, A73, doi: [10.1051/0004-6361/201117325](https://doi.org/10.1051/0004-6361/201117325)

Hildebrandt, H., Viola, M., Heymans, C., et al. 2017, MNRAS, 465, 1454, doi: [10.1093/mnras/stw2805](https://doi.org/10.1093/mnras/stw2805)

Hu, C., Du, P., Lu, K.-X., et al. 2015, ApJ, 804, 138, doi: [10.1088/0004-637X/804/2/138](https://doi.org/10.1088/0004-637X/804/2/138)

Joudaki, S., Mead, A., Blake, C., et al. 2017, MNRAS, 471, 1259, doi: [10.1093/mnras/stx998](https://doi.org/10.1093/mnras/stx998)

Kaspi, S., Smith, P. S., Netzer, H., et al. 2000, ApJ, 533, 631, doi: [10.1086/308704](https://doi.org/10.1086/308704)

Kilerci Eser, E., Vestergaard, M., Peterson, B. M., Denney, K. D., & Bentz, M. C. 2015, ApJ, 801, 8, doi: [10.1088/0004-637X/801/1/8](https://doi.org/10.1088/0004-637X/801/1/8)

King, A., & Lasota, J.-P. 2014, MNRAS, 444, L30, doi: [10.1093/mnrasl/slu105](https://doi.org/10.1093/mnrasl/slu105)

King, A. L., Martini, P., Davis, T. M., et al. 2015, MNRAS, 453, 1701, doi: [10.1093/mnras/stv1718](https://doi.org/10.1093/mnras/stv1718)

Li, Z., McGreer, I. D., Wu, X.-B., Fan, X., & Yang, Q. 2018, ApJ, 861, 6, doi: [10.3847/1538-4357/aac6ce](https://doi.org/10.3847/1538-4357/aac6ce)

Lu, K.-X., Du, P., Hu, C., et al. 2016, ApJ, 827, 118, doi: [10.3847/0004-637X/827/2/118](https://doi.org/10.3847/0004-637X/827/2/118)

MacLeod, C. L., Ivezić, Ž., Kochanek, C. S., et al. 2010, ApJ, 721, 1014, doi: [10.1088/0004-637X/721/2/1014](https://doi.org/10.1088/0004-637X/721/2/1014)

Maeder, A., & Meynet, G. 2000, A&A, 361, 159

Marziani, P., Sulentic, J. W., Zwitter, T., Dultzin-Hacyan, D., & Calvani, M. 2001, ApJ, 558, 553, doi: [10.1086/322286](https://doi.org/10.1086/322286)

Mejía-Restrepo, J. E., Lira, P., Netzer, H., Trakhtenbrot, B., & Capellupo, D. M. 2018, Nature Astronomy, 2, 63, doi: [10.1038/s41550-017-0305-z](https://doi.org/10.1038/s41550-017-0305-z)

Mushotzky, R. F., Edelson, R., Baumgartner, W., & Gandhi, P. 2011, ApJL, 743, L12, doi: [10.1088/2041-8205/743/1/L12](https://doi.org/10.1088/2041-8205/743/1/L12)

Pacaud, F., Pierre, M., Melin, J.-B., et al. 2018, A&A, 620, A10, doi: [10.1051/0004-6361/201834022](https://doi.org/10.1051/0004-6361/201834022)

Pei, L., Barth, A. J., Aldering, G. S., et al. 2014, ApJ, 795, 38, doi: [10.1088/0004-637X/795/1/38](https://doi.org/10.1088/0004-637X/795/1/38)

Peterson, B. M., Ferrarese, L., Gilbert, K. M., et al. 2004, ApJ, 613, 682, doi: [10.1086/423269](https://doi.org/10.1086/423269)

Planck Collaboration. 2013, ArXiv e-prints. <https://arxiv.org/abs/1303.5062>

—. 2016a, A&A, 594, A14, doi: [10.1051/0004-6361/201525814](https://doi.org/10.1051/0004-6361/201525814)

—. 2016b, A&A, 594, A24, doi: [10.1051/0004-6361/201525833](https://doi.org/10.1051/0004-6361/201525833)

—. 2018, arXiv e-prints. <https://arxiv.org/abs/1807.06209>

Rakshit, S., & Stalin, C. S. 2017, ApJ, 842, 96, doi: [10.3847/1538-4357/aa72f4](https://doi.org/10.3847/1538-4357/aa72f4)

Richards, G. T., Lacy, M., Storrie-Lombardi, L. J., et al. 2006, ApJS, 166, 470, doi: [10.1086/506525](https://doi.org/10.1086/506525)

Riess, A. G., Casertano, S., Yuan, W., et al. 2018, ApJ, 861, 126, doi: [10.3847/1538-4357/aac82e](https://doi.org/10.3847/1538-4357/aac82e)

Risaliti, G., & Lusso, E. 2015, ApJ, 815, 33, doi: [10.1088/0004-637X/815/1/33](https://doi.org/10.1088/0004-637X/815/1/33)

Rodríguez-Pascual, P. M., Alloin, D., Clavel, J., et al. 1997, ApJS, 110, 9, doi: [10.1086/312996](https://doi.org/10.1086/312996)

Sánchez, P., Lira, P., Cartier, R., et al. 2017, ApJ, 849, 110, doi: [10.3847/1538-4357/aa9188](https://doi.org/10.3847/1538-4357/aa9188)

Sánchez-Sáez, P., Lira, P., Mejía-Restrepo, J., et al. 2018, ApJ, 864, 87, doi: [10.3847/1538-4357/aad7f9](https://doi.org/10.3847/1538-4357/aad7f9)

Sergeev, S. G., Doroshenko, V. T., Dzyuba, S. A., et al. 2007, ApJ, 668, 708, doi: [10.1086/520697](https://doi.org/10.1086/520697)

Shakura, N. I., & Sunyaev, R. A. 1973, A&A, 24, 337

Shen, Y., & Ho, L. C. 2014, Nature, 513, 210, doi: [10.1038/nature13712](https://doi.org/10.1038/nature13712)

Shen, Y., Greene, J. E., Ho, L. C., et al. 2015, ApJ, 805, 96, doi: [10.1088/0004-637X/805/2/96](https://doi.org/10.1088/0004-637X/805/2/96)

Shen, Y., Hall, P. B., Horne, K., et al. 2018, arXiv e-prints. <https://arxiv.org/abs/1810.01447>

Simm, T., Salvato, M., Saglia, R., et al. 2016, A&A, 585, A129, doi: [10.1051/0004-6361/201527353](https://doi.org/10.1051/0004-6361/201527353)

Stanway, E. R., & Eldridge, J. J. 2019, A&A, 621, A105, doi: [10.1051/0004-6361/201834359](https://doi.org/10.1051/0004-6361/201834359)

Sulentic, J. W., del Olmo, A., Marziani, P., et al. 2017, A&A, 608, A122, doi: [10.1051/0004-6361/201630309](https://doi.org/10.1051/0004-6361/201630309)

Timmer, J., & Koenig, M. 1995, A&A, 300, 707

Uttley, P., McHardy, I. M., & Vaughan, S. 2005, MNRAS, 359, 345, doi: [10.1111/j.1365-2966.2005.08886.x](https://doi.org/10.1111/j.1365-2966.2005.08886.x)

Wang, J.-M., Du, P., Li, Y.-R., et al. 2014a, ApJL, 792, L13, doi: [10.1088/2041-8205/792/1/L13](https://doi.org/10.1088/2041-8205/792/1/L13)

Wang, J.-M., Qiu, J., Du, P., & Ho, L. C. 2014b, ApJ, 797, 65, doi: [10.1088/0004-637X/797/1/65](https://doi.org/10.1088/0004-637X/797/1/65)

Wang, J.-M., Du, P., Hu, C., et al. 2014c, ApJ, 793, 108, doi: [10.1088/0004-637X/793/2/108](https://doi.org/10.1088/0004-637X/793/2/108)

Watson, D., Denney, K. D., Vestergaard, M., & Davis, T. M. 2011, ApJL, 740, L49, doi: [10.1088/2041-8205/740/2/L49](https://doi.org/10.1088/2041-8205/740/2/L49)

Wilhite, B. C., Brunner, R. J., Grier, C. J., Schneider, D. P., & vanden Berk, D. E. 2008, MNRAS, 383, 1232, doi: [10.1111/j.1365-2966.2007.12655.x](https://doi.org/10.1111/j.1365-2966.2007.12655.x)

Woo, J.-H., Schulze, A., Park, D., et al. 2013, ApJ, 772, 49, doi: [10.1088/0004-637X/772/1/49](https://doi.org/10.1088/0004-637X/772/1/49)

Woo, J.-H., Yoon, Y., Park, S., Park, D., & Kim, S. C. 2015, ApJ, 801, 38, doi: [10.1088/0004-637X/801/1/38](https://doi.org/10.1088/0004-637X/801/1/38)

Zhang, Z.-X., Du, P., Smith, P. S., et al. 2018, arXiv e-prints. <https://arxiv.org/abs/1811.03812>

Table 1. Sample description

Object	z	$\log L_{5100}$ [erg s $^{-1}$]	τ_{obs} [days]	FWHM [km s $^{-1}$]	Reference
(1)	(2)	(3)	(4)	(5)	(6)
SEAMBH sample					
Mrk335	0.0258	43.764 ± 0.067	$14.0^{+4.6}_{-3.4}$	2096 ± 170	1
Mrk142	0.0449	43.594 ± 0.044	$6.4^{+7.3}_{-3.4}$	1588 ± 58	1
IRASF12397	0.0435	44.229 ± 0.054	$9.7^{+5.5}_{-1.8}$	1802 ± 560	1
Mrk486	0.0389	43.694 ± 0.050	$23.7^{+7.5}_{-2.7}$	1942 ± 67	2
Mrk382	0.0337	43.124 ± 0.085	$7.5^{+2.9}_{-2.0}$	1462 ± 296	2
IRAS04416	0.0889	44.467 ± 0.030	$13.3^{+13.9}_{-1.4}$	1522 ± 44	2
MCG+06-26-012	0.0328	42.675 ± 0.106	$24.0^{+8.4}_{-4.8}$	1334 ± 80	2
Mrk493	0.0313	43.112 ± 0.075	$11.6^{+1.2}_{-2.6}$	778 ± 12	2
Mrk1044	0.0165	43.095 ± 0.102	$10.5^{+3.3}_{-2.7}$	1178 ± 22	2
J080101	0.1396	44.270 ± 0.030	$8.3^{+9.7}_{-2.7}$	1930 ± 18	3
J081456	0.1197	43.990 ± 0.040	$24.3^{+7.7}_{-16.4}$	2409 ± 61	3
J093922	0.1859	44.070 ± 0.040	$11.9^{+2.1}_{-6.3}$	1209 ± 16	3
J080131	0.1786	43.950 ± 0.040	$11.5^{+7.5}_{-3.7}$	1290 ± 13	4
J085946	0.2438	44.410 ± 0.030	$34.8^{+19.2}_{-26.3}$	1718 ± 16	4
J102339	0.1364	44.090 ± 0.030	$24.9^{+19.8}_{-3.9}$	1733 ± 29	4
J074352	0.2520	45.370 ± 0.020	$43.9^{+5.2}_{-4.2}$	3156 ± 36	5
J075051	0.4004	45.330 ± 0.010	$66.6^{+18.7}_{-9.9}$	1904 ± 9	5
J075101	0.1209	44.240 ± 0.040	$30.4^{+7.3}_{-5.8}$	1679 ± 35	5
J075949	0.1879	44.190 ± 0.060	$43.9^{+33.1}_{-19.0}$	1783 ± 17	5
J081441	0.1626	43.950 ± 0.040	$25.3^{+10.4}_{-7.5}$	1782 ± 16	5
J083553	0.2051	44.440 ± 0.020	$12.4^{+5.4}_{-5.4}$	1758 ± 16	5
J084533	0.3024	44.520 ± 0.020	$18.1^{+6.0}_{-4.7}$	1297 ± 12	5
J093302	0.1772	44.310 ± 0.130	$19.0^{+3.8}_{-4.3}$	1800 ± 25	5
J100402	0.3272	45.520 ± 0.010	$32.2^{+43.5}_{-4.2}$	2088 ± 1	5
J101000	0.2564	44.760 ± 0.020	$27.7^{+23.5}_{-7.6}$	2311 ± 11	5
SDSS-RM sample					
J140812	0.1160	43.154 ± 0.013	$10.5^{+1.0}_{-2.2}$	4345 ± 558	6
J141923	0.1520	43.122 ± 0.010	$11.8^{+0.7}_{-1.5}$	2945 ± 20	6
J140759	0.1720	43.577 ± 0.009	$16.3^{+13.1}_{-6.6}$	3662 ± 27	6
J141729	0.2370	43.291 ± 0.007	$5.5^{+5.7}_{-2.1}$	9208 ± 269	6
J141645.15	0.2440	43.213 ± 0.007	$5.0^{+1.5}_{-1.4}$	7409 ± 113	6
J142135	0.2490	43.475 ± 0.007	$3.9^{+0.9}_{-0.9}$	3090 ± 66	6
J141625	0.2630	43.964 ± 0.019	$15.1^{+3.2}_{-4.6}$	3515 ± 17	6
J142103	0.2630	43.636 ± 0.019	$75.2^{+3.2}_{-3.3}$	2990 ± 48	6
J142038	0.2650	43.458 ± 0.006	$25.2^{+4.7}_{-5.7}$	4700 ± 55	6
J142043	0.3370	43.400 ± 0.005	$5.9^{+0.4}_{-0.6}$	4429 ± 105	6
J141041	0.3590	43.824 ± 0.005	$21.9^{+4.2}_{-2.4}$	5034 ± 35	6
J141318	0.3620	43.941 ± 0.005	$20.0^{+1.1}_{-3.0}$	3428 ± 37	6
J141955	0.4180	43.395 ± 0.005	$10.7^{+5.6}_{-4.4}$	6789 ± 580	6
J141645.58	0.4420	43.679 ± 0.009	$8.5^{+2.5}_{-1.4}$	2178 ± 44	6
J141324	0.4560	43.945 ± 0.004	$25.5^{+10.9}_{-5.8}$	6076 ± 121	6
J141214	0.4580	44.397 ± 0.004	$21.4^{+4.2}_{-6.4}$	2652 ± 302	6
J140518	0.4670	44.333 ± 0.004	$41.6^{+14.8}_{-8.3}$	3406 ± 22	6

J141018	0.4700	43.584 \pm 0.005	16.2 $^{+2.9}_{-4.5}$	4329 \pm 298	6
J141123	0.4720	44.128 \pm 0.004	13.0 $^{+1.4}_{-0.8}$	4106 \pm 38	6
J142039	0.4740	44.141 \pm 0.004	20.7 $^{+0.9}_{-3.0}$	4259 \pm 90	6
J141724	0.4820	43.992 \pm 0.004	10.1 $^{+12.5}_{-2.7}$	5230 \pm 76	6
J141004	0.5270	44.224 \pm 0.003	53.5 $^{+4.2}_{-4.0}$	2918 \pm 62	6
J141706	0.5320	44.186 \pm 0.003	10.4 $^{+6.3}_{-3.0}$	1682 \pm 14	6
J142010	0.5480	44.088 \pm 0.003	12.8 $^{+5.7}_{-4.5}$	6050 \pm 541	6
J141712	0.5540	43.209 \pm 0.012	12.5 $^{+1.8}_{-2.6}$	2226 \pm 405	6
J141115	0.5720	44.313 \pm 0.003	49.1 $^{+11.1}_{-2.0}$	3442 \pm 51	6
J141112	0.5870	44.123 \pm 0.003	20.4 $^{+2.5}_{-2.0}$	2765 \pm 36	6
J141417	0.6040	43.397 \pm 0.013	15.6 $^{+3.2}_{-5.1}$	6476 \pm 793	6
J141031	0.6080	44.022 \pm 0.003	35.8 $^{+1.1}_{-10.3}$	3495 \pm 118	6
J141941	0.6460	44.522 \pm 0.017	30.4 $^{+3.9}_{-8.3}$	2818 \pm 48	6
J141135	0.6500	44.040 \pm 0.004	17.6 $^{+8.6}_{-7.4}$	2515 \pm 61	6
J140904	0.6580	44.147 \pm 0.004	11.6 $^{+8.6}_{-4.6}$	10405 \pm 1094	6
J142052	0.6760	45.059 \pm 0.003	11.9 $^{+1.3}_{-1.0}$	3646 \pm 14	6
J141147	0.6800	44.025 \pm 0.004	6.4 $^{+1.5}_{-1.4}$	2338 \pm 65	6
J141532	0.7150	44.136 \pm 0.004	26.5 $^{+9.9}_{-8.8}$	1615 \pm 38	6
J142023	0.7340	44.222 \pm 0.006	8.5 $^{+3.2}_{-3.9}$	4446 \pm 135	6
J142049	0.7510	44.446 \pm 0.003	46.0 $^{+9.5}_{-9.5}$	4665 \pm 97	6
J142112	0.8430	44.315 \pm 0.008	14.2 $^{+3.7}_{-3.0}$	4428 \pm 295	6
J141606	0.8480	44.801 \pm 0.003	32.0 $^{+11.6}_{-15.5}$	7307 \pm 213	6
J141859	0.8840	44.907 \pm 0.003	20.4 $^{+5.6}_{-7.0}$	4999 \pm 53	6
J141952	0.8840	44.246 \pm 0.006	32.9 $^{+5.6}_{-5.1}$	7726 \pm 319	6
J142417	0.8900	44.089 \pm 0.060	36.3 $^{+4.5}_{-5.5}$	1721 \pm 147	6
J141856 [†]	0.9760	45.382 \pm 0.002	15.8 $^{+6.0}_{-1.9}$	3120 \pm 58	6 [†]
J141314 [†]	1.0260	44.524 \pm 0.038	43.9 $^{+4.9}_{-4.3}$	1412 \pm 183	6 [†]

Bentz collection

PG0026+129	0.1420	44.970 \pm 0.016	111.0 $^{+24.1}_{-28.3}$	1719 \pm 495	7
PG0052+251	0.1545	44.807 \pm 0.025	89.8 $^{+24.5}_{-24.1}$	4165 \pm 381	7
Fairall9	0.0470	43.981 \pm 0.041	17.4 $^{+3.2}_{-4.3}$	6901 \pm 707	7
Mrk590	0.0264	43.496 \pm 0.212	25.6 $^{+6.5}_{-5.3}$	2220 \pm 701	7
3C120	0.0330	44.004 \pm 0.100	26.2 $^{+8.7}_{-6.6}$	2372 \pm 501	7
Ark120	0.0327	43.867 \pm 0.253	39.5 $^{+8.5}_{-7.8}$	5410 \pm 360	7
Mrk79	0.0222	43.677 \pm 0.067	15.6 $^{+5.4}_{-4.9}$	4852 \pm 1554	7
PG0804+761	0.1000	44.910 \pm 0.017	146.9 $^{+18.8}_{-18.9}$	2012 \pm 845	7
Mrk110	0.0353	43.658 \pm 0.115	25.6 $^{+8.9}_{-7.2}$	1494 \pm 802	7
PG0953+414	0.2341	45.186 \pm 0.013	150.1 $^{+21.6}_{-22.6}$	3002 \pm 398	7
NGC3227	0.0039	42.236 \pm 0.106	3.8 $^{+0.8}_{-0.8}$	3578 \pm 83	7
NGC3516	0.0088	42.787 \pm 0.205	11.7 $^{+1.0}_{-1.5}$	5175 \pm 96	7
SBS1116+583A	0.0279	42.138 \pm 0.231	2.3 $^{+0.6}_{-0.5}$	3604 \pm 1123	7
Arp151	0.0211	42.548 \pm 0.101	4.0 $^{+0.5}_{-0.7}$	2357 \pm 142	7
NGC3783	0.0097	42.558 \pm 0.180	10.2 $^{+3.3}_{-2.3}$	3093 \pm 529	7
Mrk1310	0.0196	42.293 \pm 0.145	3.7 $^{+0.6}_{-0.6}$	1602 \pm 250	7
NGC4051	0.0023	41.898 \pm 0.152	2.1 $^{+0.9}_{-0.7}$	1034 \pm 41	7
NGC4151	0.0033	42.091 \pm 0.207	6.6 $^{+1.1}_{-0.8}$	4711 \pm 750	7
Mrk202	0.0210	42.260 \pm 0.144	3.0 $^{+1.7}_{-1.1}$	1354 \pm 250	7
NGC4253	0.0129	42.570 \pm 0.122	6.2 $^{+1.6}_{-1.2}$	834 \pm 1260	7
PG1229+204	0.0630	43.697 \pm 0.047	37.8 $^{+27.6}_{-15.3}$	3415 \pm 320	7
NGC4593	0.0090	42.621 \pm 0.370	4.0 $^{+0.8}_{-0.7}$	4268 \pm 551	7

NGC4748	0.0146	42.556 ± 0.120	$5.5^{+1.6}_{-2.2}$	1212 ± 173	7
PG1307+085	0.1550	44.849 ± 0.015	$105.6^{+36.0}_{-46.6}$	5058 ± 524	7
Mrk279	0.0305	43.705 ± 0.074	$16.7^{+3.9}_{-3.9}$	3385 ± 349	7
PG1411+442	0.0896	44.563 ± 0.020	$124.3^{+61.0}_{-61.7}$	2398 ± 353	7
PG1426+015	0.0866	44.629 ± 0.024	$95.0^{+29.9}_{-37.1}$	6323 ± 1295	7
Mrk817	0.0315	43.743 ± 0.089	$19.9^{+9.9}_{-6.7}$	4122 ± 1197	7
Mrk290	0.0296	43.168 ± 0.057	$8.7^{+1.2}_{-1.0}$	4270 ± 157	7
PG1613+658	0.1290	44.774 ± 0.022	$40.1^{+15.0}_{-15.2}$	7897 ± 1792	7
PG1617+175	0.1124	44.391 ± 0.017	$71.5^{+29.6}_{-33.7}$	4718 ± 991	7
PG1700+518	0.2920	45.586 ± 0.007	$251.8^{+45.9}_{-38.8}$	1846 ± 682	7
3C390.3	0.0561	44.434 ± 0.576	$44.5^{+27.7}_{-17.0}$	10415 ± 1971	7
NGC6814	0.0052	42.120 ± 0.285	$6.6^{+0.9}_{-0.9}$	3277 ± 297	7
Mrk509	0.0344	44.193 ± 0.045	$79.6^{+6.1}_{-5.4}$	2715 ± 101	7
PG2130+099	0.0630	44.203 ± 0.028	$9.6^{+1.2}_{-1.2}$	2097 ± 102	7
NGC7469	0.0163	43.506 ± 0.108	$10.8^{+3.4}_{-1.3}$	1066 ± 84	7
PG1211+143	0.0809	44.728 ± 0.081	$93.8^{+25.6}_{-42.1}$	2012 ± 37	8
PG0844+349	0.0640	44.218 ± 0.071	$32.3^{+13.7}_{-13.4}$	2436 ± 329	8
NGC5273	0.0036	41.535 ± 0.160	$2.2^{+1.2}_{-1.6}$	4615 ± 330	9
Mrk1511	0.0339	43.162 ± 0.062	$5.7^{+0.9}_{-0.8}$	4171 ± 137	10
KA1858-4850	0.0780	43.428 ± 0.047	$13.5^{+2.0}_{-2.3}$	1511 ± 68	11
MCG6-30-15	0.0078	41.643 ± 0.108	$5.7^{+1.8}_{-1.7}$	1422 ± 416	12
UGC06728	0.0065	41.864 ± 0.081	$1.4^{+0.7}_{-0.8}$	1145 ± 58	13
MCG+08-11-011	0.0205	43.330 ± 0.111	$15.7^{+0.5}_{-0.5}$	1159 ± 8	14
NGC2617	0.0142	42.667 ± 0.159	$4.3^{+1.1}_{-1.4}$	5303 ± 49	14
3C382	0.0579	43.835 ± 0.102	$40.5^{+8.0}_{-3.7}$	3619 ± 282	14
Mrk374	0.0426	43.774 ± 0.042	$14.8^{+5.8}_{-3.3}$	3250 ± 19	14
Lu et al. (2016)					
NGC5548	0.0172	43.210 ± 0.120	$7.2^{+1.3}_{-0.4}$	9912 ± 362	15
Zhang et al. (2018)					
3C273	0.1583	45.965 ± 0.016	$146.8^{+8.3}_{-12.1}$	3314 ± 59	16

NOTES. Columns are as follows: (1) Object name. Discarded object of the analysis are marked by † symbol. (2) Redshift. (3) Luminosity at 5100 Å. (4) Delay time at rest-frame. (5) FWHM of H β emission line. (6) References: 1: Du et al. (2014), 2: Wang et al. (2014c), 3: Du et al. (2015), 4: Du et al. (2016), 5: Du et al. (2018), 6: Grier et al. (2017), 7: Bentz et al. (2013), 8: Bentz et al. (2009), 9: Bentz et al. (2014), 10: Barth et al. (2013), 11: Pei et al. (2014), 12: Bentz et al. (2016a), 13: Bentz et al. (2016b), 14: Fausnaugh et al. (2017), 15: Lu et al. (2016), 16: Zhang et al. (2018).

Table 2. Observational properties for the full sample

Object	$\log M_{\text{BH}}$ [M_{\odot}]	$\log \dot{M}$	$L_{\text{bol}}/L_{\text{Edd}}$	$\log \Delta R_{H\beta}$	f_{BLR}^c	F_{var}
(1)	(2)	(3)	(4)	(5)	(6)	(7)
SEAMBH sample						
Mrk335	$7.08^{+0.16}_{-0.13}$	$0.97^{+0.33}_{-0.27}$	$0.33^{+0.15}_{-0.13}$	$-0.25^{+0.15}_{-0.12}$	2.48 ± 0.24	0.030 ¹
Mrk142	$6.50^{+0.50}_{-0.23}$	$1.88^{+0.99}_{-0.47}$	$0.85^{+1.00}_{-0.50}$	$-0.50^{+0.50}_{-0.23}$	3.43 ± 0.15	0.066 ¹
IRASF12397	$6.79^{+0.37}_{-0.28}$	$2.25^{+0.74}_{-0.57}$	$1.89^{+1.65}_{-1.30}$	$-0.66^{+0.25}_{-0.09}$	2.96 ± 1.07	0.041 ¹
Mrk486	$7.24^{+0.14}_{-0.06}$	$0.54^{+0.29}_{-0.14}$	$0.19^{+0.08}_{-0.05}$	$0.01^{+0.14}_{-0.07}$	2.71 ± 0.11	0.034 ¹
Mrk382	$6.50^{+0.24}_{-0.21}$	$1.18^{+0.50}_{-0.44}$	$0.29^{+0.18}_{-0.16}$	$-0.18^{+0.18}_{-0.13}$	3.77 ± 0.89	0.041 ¹
IRAS04416	$6.78^{+0.45}_{-0.05}$	$2.63^{+0.91}_{-0.11}$	$3.34^{+3.57}_{-0.82}$	$-0.65^{+0.46}_{-0.06}$	3.60 ± 0.12	0.020 ¹
MCG06	$6.92^{+0.16}_{-0.10}$	$-0.34^{+0.36}_{-0.26}$	$0.04^{+0.02}_{-0.02}$	$0.56^{+0.17}_{-0.12}$	4.20 ± 0.29	0.092 ¹
Mrk493	$6.14^{+0.05}_{-0.10}$	$1.88^{+0.15}_{-0.23}$	$0.65^{+0.19}_{-0.23}$	$0.01^{+0.07}_{-0.11}$	7.90 ± 0.14	0.031 ¹
Mrk1044	$6.46^{+0.14}_{-0.11}$	$1.22^{+0.31}_{-0.27}$	$0.30^{+0.13}_{-0.12}$	$-0.02^{+0.15}_{-0.13}$	4.86 ± 0.11	0.037 ¹
J080101	$6.78^{+0.51}_{-0.14}$	$2.33^{+1.02}_{-0.29}$	$2.12^{+2.51}_{-0.82}$	$-0.75^{+0.51}_{-0.15}$	2.73 ± 0.03	0.039
J081456	$7.44^{+0.14}_{-0.29}$	$0.59^{+0.29}_{-0.59}$	$0.24^{+0.09}_{-0.17}$	$-0.14^{+0.14}_{-0.30}$	2.10 ± 0.06	0.031
J093922	$6.53^{+0.08}_{-0.23}$	$2.53^{+0.17}_{-0.46}$	$2.37^{+0.67}_{-1.36}$	$-0.49^{+0.09}_{-0.23}$	4.71 ± 0.07	0.036
J080131	$6.57^{+0.29}_{-0.14}$	$2.27^{+0.57}_{-0.29}$	$1.64^{+1.14}_{-0.64}$	$-0.44^{+0.29}_{-0.15}$	4.37 ± 0.05	0.047
J085946	$7.30^{+0.24}_{-0.33}$	$1.50^{+0.48}_{-0.66}$	$0.88^{+0.52}_{-0.69}$	$-0.14^{+0.14}_{-0.30}$	3.13 ± 0.03	0.048
J102339	$7.17^{+0.35}_{-0.07}$	$1.29^{+0.69}_{-0.15}$	$0.58^{+0.48}_{-0.15}$	$-0.18^{+0.35}_{-0.08}$	3.09 ± 0.06	0.032
J074352	$7.93^{+0.05}_{-0.04}$	$1.68^{+0.11}_{-0.09}$	$1.88^{+0.45}_{-0.43}$	$-0.61^{+0.08}_{-0.07}$	1.53 ± 0.02	0.060
J075051	$7.68^{+0.12}_{-0.06}$	$2.14^{+0.24}_{-0.13}$	$3.11^{+1.08}_{-0.78}$	$-0.41^{+0.13}_{-0.08}$	2.77 ± 0.02	0.032
J075101	$7.22^{+0.11}_{-0.08}$	$1.40^{+0.22}_{-0.18}$	$0.71^{+0.23}_{-0.21}$	$-0.17^{+0.11}_{-0.09}$	3.21 ± 0.08	0.065
J075949	$7.44^{+0.33}_{-0.19}$	$0.90^{+0.66}_{-0.39}$	$0.39^{+0.31}_{-0.19}$	$0.01^{+0.33}_{-0.19}$	2.99 ± 0.03	0.094
J081441	$7.20^{+0.18}_{-0.13}$	$1.02^{+0.36}_{-0.27}$	$0.39^{+0.18}_{-0.14}$	$-0.10^{+0.18}_{-0.13}$	2.99 ± 0.03	0.051
J083553	$6.88^{+0.19}_{-0.19}$	$2.40^{+0.38}_{-0.38}$	$2.53^{+1.22}_{-1.22}$	$-0.67^{+0.19}_{-0.19}$	3.04 ± 0.03	0.052
J084533	$6.78^{+0.14}_{-0.11}$	$2.72^{+0.29}_{-0.23}$	$3.82^{+1.49}_{-1.27}$	$-0.55^{+0.15}_{-0.12}$	4.34 ± 0.05	0.040
J093302	$7.08^{+0.09}_{-0.10}$	$1.79^{+0.26}_{-0.28}$	$1.17^{+0.48}_{-0.50}$	$-0.41^{+0.12}_{-0.12}$	2.96 ± 0.05	0.036
J100402	$7.44^{+0.59}_{-0.06}$	$2.89^{+1.17}_{-0.11}$	$8.29^{+11.32}_{-2.00}$	$-0.83^{+0.59}_{-0.08}$	2.49 ± 0.001	0.048
J101000	$7.46^{+0.37}_{-0.12}$	$1.71^{+0.74}_{-0.24}$	$1.37^{+1.19}_{-0.47}$	$-0.49^{+0.37}_{-0.13}$	2.21 ± 0.001	0.065
SDSS sample						
J140812	$7.59^{+0.12}_{-0.14}$	$-0.96^{+0.24}_{-0.29}$	$0.03^{+0.01}_{-0.01}$	$-0.05^{+0.06}_{-0.10}$	1.06 ± 0.16	0.043
J141923	$7.30^{+0.03}_{-0.06}$	$-0.43^{+0.06}_{-0.11}$	$0.05^{+0.01}_{-0.01}$	$0.01^{+0.05}_{-0.07}$	1.66 ± 0.01	0.076
J140759	$7.63^{+0.35}_{-0.18}$	$-0.41^{+0.70}_{-0.35}$	$0.06^{+0.05}_{-0.03}$	$-0.09^{+0.35}_{-0.18}$	1.29 ± 0.01	0.038
J141729	$7.96^{+0.45}_{-0.17}$	$-1.49^{+0.90}_{-0.34}$	$0.01^{+0.02}_{-0.01}$	$-0.41^{+0.45}_{-0.17}$	0.44 ± 0.01	0.033
J141645.15	$7.73^{+0.13}_{-0.12}$	$-1.15^{+0.26}_{-0.24}$	$0.02^{+0.01}_{-0.01}$	$-0.41^{+0.14}_{-0.13}$	0.57 ± 0.01	0.068
J142135	$6.86^{+0.10}_{-0.10}$	$0.98^{+0.20}_{-0.20}$	$0.28^{+0.09}_{-0.09}$	$-0.66^{+0.11}_{-0.11}$	1.57 ± 0.04	0.038
J141625	$7.56^{+0.09}_{-0.13}$	$0.31^{+0.19}_{-0.27}$	$0.17^{+0.05}_{-0.06}$	$-0.33^{+0.10}_{-0.14}$	1.35 ± 0.01	0.058
J142103	$8.12^{+0.02}_{-0.02}$	$-1.30^{+0.05}_{-0.06}$	$0.02^{+0.005}_{-0.005}$	$0.54^{+0.04}_{-0.04}$	1.63 ± 0.03	–
J142038	$8.04^{+0.08}_{-0.10}$	$-1.40^{+0.16}_{-0.20}$	$0.02^{+0.01}_{-0.01}$	$0.16^{+0.09}_{-0.10}$	0.96 ± 0.01	0.065
J142043	$7.36^{+0.04}_{-0.05}$	$-0.12^{+0.07}_{-0.10}$	$0.08^{+0.02}_{-0.02}$	$-0.44^{+0.05}_{-0.06}$	1.03 ± 0.03	0.036
J141041	$8.04^{+0.08}_{-0.05}$	$-0.85^{+0.17}_{-0.10}$	$0.04^{+0.01}_{-0.01}$	$-0.09^{+0.09}_{-0.06}$	0.89 ± 0.01	0.074
J141318	$7.66^{+0.03}_{-0.07}$	$0.08^{+0.05}_{-0.13}$	$0.13^{+0.03}_{-0.03}$	$-0.19^{+0.04}_{-0.07}$	1.39 ± 0.02	0.060
J141955	$7.99^{+0.24}_{-0.19}$	$-1.39^{+0.48}_{-0.39}$	$0.02^{+0.01}_{-0.01}$	$-0.18^{+0.23}_{-0.18}$	0.63 ± 0.06	0.066
J141645.58	$6.90^{+0.13}_{-0.07}$	$1.21^{+0.26}_{-0.15}$	$0.42^{+0.15}_{-0.11}$	$-0.43^{+0.13}_{-0.08}$	2.37 ± 0.06	0.053
J141324	$8.27^{+0.19}_{-0.10}$	$-1.12^{+0.37}_{-0.20}$	$0.03^{+0.02}_{-0.01}$	$-0.09^{+0.19}_{-0.10}$	0.71 ± 0.02	0.046
J141214	$7.47^{+0.13}_{-0.16}$	$1.15^{+0.26}_{-0.33}$	$0.58^{+0.21}_{-0.25}$	$-0.41^{+0.09}_{-0.13}$	1.88 ± 0.25	0.034
J140518	$7.98^{+0.15}_{-0.09}$	$0.04^{+0.31}_{-0.17}$	$0.16^{+0.06}_{-0.04}$	$-0.09^{+0.16}_{-0.09}$	1.40 ± 0.01	0.072

J141018	7.77 ^{+0.10} _{-0.13}	-0.68 ^{+0.20} _{-0.27}	0.04 ^{+0.01} _{-0.02}	-0.10 ^{+0.08} _{-0.13}	1.06 ± 0.09	0.044
J141123	7.63 ^{+0.05} _{-0.03}	0.42 ^{+0.10} _{-0.06}	0.22 ^{+0.05} _{-0.05}	-0.48 ^{+0.06} _{-0.04}	1.13 ± 0.01	0.071
J142039	7.87 ^{+0.03} _{-0.07}	-0.03 ^{+0.05} _{-0.13}	0.13 ^{+0.03} _{-0.03}	-0.29 ^{+0.04} _{-0.07}	1.08 ± 0.03	0.079
J141724	7.73 ^{+0.54} _{-0.12}	0.01 ^{+1.08} _{-0.23}	0.12 ^{+0.16} _{-0.04}	-0.52 ^{+0.54} _{-0.12}	0.85 ± 0.01	0.064
J141004	7.95 ^{+0.04} _{-0.04}	-0.08 ^{+0.08} _{-0.07}	0.13 ^{+0.03} _{-0.03}	0.08 ^{+0.05} _{-0.05}	1.68 ± 0.04	0.028
J141706	6.76 ^{+0.26} _{-0.13}	2.25 ^{+0.53} _{-0.25}	1.83 ^{+1.17} _{-0.65}	-0.61 ^{+0.26} _{-0.13}	3.20 ± 0.03	0.052
J142010	7.96 ^{+0.21} _{-0.17}	-0.30 ^{+0.42} _{-0.34}	0.09 ^{+0.05} _{-0.04}	-0.47 ^{+0.20} _{-0.16}	0.72 ± 0.08	0.133
J141712	7.08 ^{+0.17} _{-0.18}	0.14 ^{+0.34} _{-0.36}	0.09 ^{+0.04} _{-0.04}	-0.01 ^{+0.08} _{-0.10}	2.31 ± 0.49	0.189
J141115	8.06 ^{+0.10} _{-0.02}	-0.15 ^{+0.20} _{-0.04}	0.12 ^{+0.04} _{-0.03}	0.003 ^{+0.10} _{-0.04}	1.39 ± 0.02	0.064
J141112	7.49 ^{+0.05} _{-0.04}	0.70 ^{+0.11} _{-0.09}	0.30 ^{+0.07} _{-0.07}	-0.28 ^{+0.06} _{-0.05}	1.79 ± 0.03	0.037
J141417	8.11 ^{+0.14} _{-0.18}	-1.63 ^{+0.28} _{-0.36}	0.01 ^{+0.01} _{-0.01}	-0.01 ^{+0.10} _{-0.15}	0.66 ± 0.09	0.149
J141031	7.93 ^{+0.03} _{-0.13}	-0.34 ^{+0.06} _{-0.26}	0.08 ^{+0.02} _{-0.03}	0.02 ^{+0.03} _{-0.13}	1.36 ± 0.05	0.053
J141941	7.68 ^{+0.06} _{-0.12}	0.92 ^{+0.12} _{-0.24}	0.48 ^{+0.12} _{-0.17}	-0.32 ^{+0.07} _{-0.12}	1.75 ± 0.03	0.055
J141135	7.34 ^{+0.21} _{-0.18}	0.87 ^{+0.43} _{-0.37}	0.35 ^{+0.18} _{-0.16}	-0.30 ^{+0.21} _{-0.19}	2.00 ± 0.06	0.096
J140904	8.39 ^{+0.33} _{-0.19}	-1.07 ^{+0.67} _{-0.39}	0.04 ^{+0.03} _{-0.02}	-0.54 ^{+0.32} _{-0.18}	0.38 ± 0.05	0.099
J142052	7.49 ^{+0.05} _{-0.04}	2.10 ^{+0.10} _{-0.07}	2.54 ^{+0.58} _{-0.56}	-1.02 ^{+0.07} _{-0.06}	1.30 ± 0.01	0.022
J141147	6.84 ^{+0.10} _{-0.10}	1.86 ^{+0.21} _{-0.20}	1.06 ^{+0.33} _{-0.32}	-0.73 ^{+0.11} _{-0.10}	2.18 ± 0.07	0.092
J141532	7.13 ^{+0.16} _{-0.15}	1.43 ^{+0.33} _{-0.29}	0.70 ^{+0.30} _{-0.27}	-0.18 ^{+0.17} _{-0.15}	3.36 ± 0.09	0.274
J142023	7.52 ^{+0.17} _{-0.20}	0.79 ^{+0.33} _{-0.40}	0.35 ^{+0.15} _{-0.18}	-0.72 ^{+0.17} _{-0.20}	1.03 ± 0.04	0.107
J142049	8.29 ^{+0.09} _{-0.09}	-0.43 ^{+0.18} _{-0.18}	0.10 ^{+0.03} _{-0.03}	-0.10 ^{+0.10} _{-0.10}	0.97 ± 0.02	0.097
J142112	7.74 ^{+0.13} _{-0.11}	0.49 ^{+0.25} _{-0.22}	0.26 ^{+0.09} _{-0.08}	-0.54 ^{+0.12} _{-0.10}	1.03 ± 0.08	0.075
J141606	8.52 ^{+0.16} _{-0.21}	-0.36 ^{+0.32} _{-0.42}	0.13 ^{+0.05} _{-0.07}	-0.45 ^{+0.16} _{-0.21}	0.57 ± 0.02	0.071
J141859	8.00 ^{+0.12} _{-0.15}	0.85 ^{+0.24} _{-0.30}	0.56 ^{+0.19} _{-0.22}	-0.70 ^{+0.13} _{-0.16}	0.90 ± 0.01	0.056
J141952	8.59 ^{+0.08} _{-0.08}	-1.31 ^{+0.16} _{-0.15}	0.03 ^{+0.01} _{-0.01}	-0.14 ^{+0.08} _{-0.07}	0.54 ± 0.03	0.166
J142417	7.32 ^{+0.09} _{-0.10}	0.98 ^{+0.20} _{-0.22}	0.40 ^{+0.13} _{-0.13}	-0.01 ^{+0.07} _{-0.08}	3.12 ± 0.31	0.275
J141856 [†]	7.48 ^{+0.17} _{-0.05}	2.60 ^{+0.33} _{-0.11}	5.50 ^{+2.37} _{-1.31}	-1.06 ^{+0.17} _{-0.08}	1.56 ± 0.03	0.144
J141314 [†]	7.23 ^{+0.12} _{-0.12}	1.81 ^{+0.25} _{-0.25}	1.34 ^{+0.48} _{-0.47}	-0.16 ^{+0.06} _{-0.06}	3.93 ± 0.60	0.216

Bentz collection

PG0026+129	7.81 ^{+0.27} _{-0.27}	1.33 ^{+0.44} _{-0.55}	1.00 ^{+0.65} _{-0.66}	0.001 ^{+0.11} _{-0.12}	3.12 ± 1.05	0.173 ²
PG0052+251	8.48 ^{+0.14} _{-0.14}	-0.27 ^{+0.43} _{-0.28}	0.14 ^{+0.06} _{-0.06}	-0.004 ^{+0.13} _{-0.12}	1.11 ± 0.12	0.199 ²
Fairall9	8.21 ^{+0.12} _{-0.14}	-0.96 ^{+0.50} _{-0.29}	0.04 ^{+0.01} _{-0.02}	-0.28 ^{+0.09} _{-0.11}	0.61 ± 0.07	0.328 ²
Mrk590	7.39 ^{+0.30} _{-0.29}	-0.05 ^{+0.43} _{-0.66}	0.09 ^{+0.08} _{-0.07}	0.15 ^{+0.16} _{-0.15}	2.32 ± 0.86	0.108 ²
3C120	7.46 ^{+0.23} _{-0.21}	0.58 ^{+0.40} _{-0.45}	0.24 ^{+0.15} _{-0.14}	-0.11 ^{+0.16} _{-0.13}	2.14 ± 0.53	0.178 ²
Ark120	8.36 ^{+0.11} _{-0.10}	-1.42 ^{+0.43} _{-0.43}	0.02 ^{+0.01} _{-0.01}	0.14 ^{+0.17} _{-0.16}	0.82 ± 0.06	0.072 ²
Mrk79	7.86 ^{+0.32} _{-0.31}	-0.71 ^{+0.43} _{-0.63}	0.05 ^{+0.04} _{-0.03}	-0.16 ^{+0.16} _{-0.14}	0.93 ± 0.35	0.091 ²
PG0804+761	8.07 ^{+0.37} _{-0.37}	0.72 ^{+0.43} _{-0.74}	0.48 ^{+0.42} _{-0.42}	0.16 ^{+0.07} _{-0.07}	2.60 ± 1.28	0.176 ²
Mrk110	7.05 ^{+0.49} _{-0.48}	0.88 ^{+0.43} _{-0.98}	0.28 ^{+0.33} _{-0.32}	0.06 ^{+0.17} _{-0.14}	3.68 ± 2.31	0.184 ²
PG0953+414	8.42 ^{+0.13} _{-0.13}	0.42 ^{+0.44} _{-0.27}	0.40 ^{+0.14} _{-0.15}	0.02 ^{+0.08} _{-0.08}	1.63 ± 0.25	0.136 ²
NGC3227	6.98 ^{+0.09} _{-0.09}	-1.11 ^{+0.43} _{-0.25}	0.01 ^{+0.005} _{-0.005}	-0.01 ^{+0.13} _{-0.13}	1.32 ± 0.04	0.094 ²
NGC3516	7.79 ^{+0.04} _{-0.06}	-1.90 ^{+0.45} _{-0.33}	0.01 ^{+0.004} _{-0.004}	0.19 ^{+0.13} _{-0.13}	0.86 ± 0.02	0.289 ²
SBS1116+583A	6.77 ^{+0.29} _{-0.29}	-0.84 ^{+0.43} _{-0.67}	0.02 ^{+0.01} _{-0.01}	-0.17 ^{+0.18} _{-0.17}	1.31 ± 0.48	0.043 ³
Arp151	6.64 ^{+0.08} _{-0.09}	0.03 ^{+0.48} _{-0.24}	0.06 ^{+0.02} _{-0.02}	-0.15 ^{+0.10} _{-0.11}	2.16 ± 0.15	0.120 ³
NGC3783	7.28 ^{+0.20} _{-0.18}	-1.24 ^{+0.40} _{-0.45}	0.01 ^{+0.01} _{-0.01}	0.25 ^{+0.18} _{-0.15}	1.57 ± 0.31	0.192 ²
Mrk1310	6.27 ^{+0.15} _{-0.15}	0.39 ^{+0.43} _{-0.37}	0.07 ^{+0.04} _{-0.04}	-0.05 ^{+0.12} _{-0.12}	3.39 ± 0.62	0.051 ³
NGC4051	5.64 ^{+0.19} _{-0.15}	1.05 ^{+0.37} _{-0.38}	0.12 ^{+0.07} _{-0.07}	-0.08 ^{+0.22} _{-0.18}	5.66 ± 0.26	0.059 ²
NGC4151	7.46 ^{+0.16} _{-0.15}	-2.29 ^{+0.42} _{-0.43}	0.003 ^{+0.002} _{-0.002}	0.31 ^{+0.15} _{-0.14}	0.96 ± 0.18	0.058 ²
Mrk202	6.03 ^{+0.29} _{-0.23}	0.82 ^{+0.35} _{-0.50}	0.12 ^{+0.09} _{-0.08}	-0.12 ^{+0.27} _{-0.19}	4.13 ± 0.89	0.027 ³
NGC4253	5.93 ^{+1.32} _{-1.31}	1.49 ^{+0.43} _{-2.64}	0.30 ^{+0.92} _{-0.92}	0.03 ^{+0.14} _{-0.12}	7.28 ± 12.87	0.053 ³
PG1229+204	7.94 ^{+0.33} _{-0.19}	-0.84 ^{+0.26} _{-0.39}	0.04 ^{+0.03} _{-0.02}	0.21 ^{+0.32} _{-0.18}	1.40 ± 0.15	0.107 ²
NGC4593	7.15 ^{+0.14} _{-0.14}	-0.89 ^{+0.43} _{-0.62}	0.02 ^{+0.02} _{-0.02}	-0.19 ^{+0.22} _{-0.22}	1.08 ± 0.16	0.114 ²

NGC4748	6.20 ^{+0.18} _{-0.21}	0.93 ^{+0.51} _{-0.47}	0.16 ^{+0.08} _{-0.09}	-0.02 ^{+0.15} _{-0.20}	4.70 ± 0.79	0.045 ³
PG1307+085	8.72 ^{+0.17} _{-0.21}	-0.68 ^{+0.53} _{-0.42}	0.09 ^{+0.04} _{-0.05}	0.04 ^{+0.15} _{-0.20}	0.88 ± 0.11	0.113 ²
Mrk279	7.57 ^{+0.14} _{-0.14}	-0.10 ^{+0.43} _{-0.29}	0.09 ^{+0.04} _{-0.04}	-0.15 ^{+0.11} _{-0.11}	1.41 ± 0.17	0.082 ²
PG1411+442	8.15 ^{+0.25} _{-0.25}	0.04 ^{+0.44} _{-0.50}	0.18 ^{+0.11} _{-0.11}	0.27 ^{+0.22} _{-0.22}	2.12 ± 0.36	0.105 ²
PG1426+015	8.87 ^{+0.22} _{-0.25}	-1.31 ^{+0.48} _{-0.49}	0.04 ^{+0.02} _{-0.02}	0.12 ^{+0.14} _{-0.17}	0.68 ± 0.16	0.173 ²
Mrk817	7.82 ^{+0.33} _{-0.29}	-0.54 ^{+0.38} _{-0.60}	0.06 ^{+0.05} _{-0.04}	-0.09 ^{+0.22} _{-0.16}	1.12 ± 0.38	0.050 ⁴
Mrk290	7.49 ^{+0.07} _{-0.06}	-0.74 ^{+0.40} _{-0.15}	0.03 ^{+0.01} _{-0.01}	-0.14 ^{+0.08} _{-0.07}	1.08 ± 0.05	0.180 ⁴
PG1613+658	8.69 ^{+0.26} _{-0.26}	-0.73 ^{+0.44} _{-0.51}	0.08 ^{+0.05} _{-0.05}	-0.34 ^{+0.17} _{-0.17}	0.52 ± 0.14	0.123 ²
PG1617+175	8.49 ^{+0.26} _{-0.27}	-0.91 ^{+0.46} _{-0.55}	0.05 ^{+0.03} _{-0.04}	0.12 ^{+0.18} _{-0.21}	0.96 ± 0.24	0.191 ²
PG1700+518	8.23 ^{+0.33} _{-0.33}	1.42 ^{+0.43} _{-0.66}	1.58 ^{+1.24} _{-1.23}	0.03 ^{+0.10} _{-0.09}	2.87 ± 1.24	0.060 ²
3C390.3	8.98 ^{+0.32} _{-0.23}	-1.81 ^{+0.40} _{-0.98}	0.02 ^{+0.03} _{-0.03}	-0.11 ^{+0.41} _{-0.35}	0.38 ± 0.08	0.343 ²
NGC6814	7.14 ^{+0.10} _{-0.10}	-1.62 ^{+0.43} _{-0.47}	0.01 ^{+0.005} _{-0.005}	0.29 ^{+0.18} _{-0.18}	1.47 ± 0.16	0.068 ³
Mrk509	8.06 ^{+0.05} _{-0.04}	-0.34 ^{+0.42} _{-0.11}	0.09 ^{+0.02} _{-0.02}	0.27 ^{+0.05} _{-0.05}	1.83 ± 0.08	0.181 ²
PG2130+099	6.92 ^{+0.07} _{-0.07}	1.96 ^{+0.43} _{-0.14}	1.33 ^{+0.35} _{-0.35}	-0.65 ^{+0.06} _{-0.06}	2.48 ± 0.14	0.086 ²
NGC7469	6.38 ^{+0.15} _{-0.09}	1.99 ^{+0.30} _{-0.24}	0.92 ^{+0.44} _{-0.35}	-0.23 ^{+0.15} _{-0.09}	5.46 ± 0.50	0.150 ²
PG1211+143	7.87 ^{+0.12} _{-0.20}	0.84 ^{+0.66} _{-0.41}	0.50 ^{+0.19} _{-0.26}	0.06 ^{+0.13} _{-0.20}	2.60 ± 0.06	0.134 ²
PG0844+349	7.57 ^{+0.22} _{-0.21}	0.67 ^{+0.43} _{-0.44}	0.30 ^{+0.17} _{-0.17}	-0.13 ^{+0.19} _{-0.19}	2.08 ± 0.33	0.105 ²
NGC5273	6.96 ^{+0.24} _{-0.32}	-2.13 ^{+0.55} _{-0.69}	0.003 ^{+0.002} _{-0.002}	0.13 ^{+0.27} _{-0.34}	0.98 ± 0.08	0.059 ⁵
Mrk1511	7.29 ^{+0.07} _{-0.07}	-0.34 ^{+0.41} _{-0.17}	0.05 ^{+0.02} _{-0.02}	-0.32 ^{+0.09} _{-0.08}	1.11 ± 0.04	0.150 ⁶
KA1858-4850	6.78 ^{+0.08} _{-0.08}	1.07 ^{+0.48} _{-0.18}	0.31 ^{+0.09} _{-0.09}	-0.09 ^{+0.08} _{-0.09}	3.63 ± 0.19	0.084 ⁷
MCG6-30-15	6.35 ^{+0.29} _{-0.28}	-0.75 ^{+0.43} _{-0.59}	0.01 ^{+0.01} _{-0.01}	0.49 ^{+0.17} _{-0.16}	3.90 ± 1.34	0.132 ⁸
UGC06728	5.56 ^{+0.22} _{-0.25}	1.17 ^{+0.49} _{-0.52}	0.14 ^{+0.08} _{-0.09}	-0.24 ^{+0.24} _{-0.26}	5.03 ± 0.30	0.090 ⁹
MCG+08-11-011	6.62 ^{+0.02} _{-0.02}	1.25 ^{+0.43} _{-0.17}	0.36 ^{+0.12} _{-0.12}	0.03 ^{+0.07} _{-0.07}	4.95 ± 0.04	0.100 ¹⁰
NGC2617	7.37 ^{+0.11} _{-0.14}	-1.26 ^{+0.48} _{-0.36}	0.01 ^{+0.01} _{-0.01}	-0.18 ^{+0.15} _{-0.17}	0.84 ± 0.01	0.090 ¹⁰
3C382	8.02 ^{+0.11} _{-0.04}	-0.79 ^{+0.28} _{-0.17}	0.05 ^{+0.02} _{-0.01}	0.17 ^{+0.11} _{-0.07}	1.31 ± 0.12	0.090 ¹⁰
Mrk374	7.49 ^{+0.17} _{-0.10}	0.18 ^{+0.26} _{-0.20}	0.13 ^{+0.06} _{-0.04}	-0.24 ^{+0.17} _{-0.10}	1.48 ± 0.01	0.030 ¹⁰
Lu et al. (2016)						
NGC5548	8.14 ^{+0.08} _{-0.04}	-1.98 ^{+0.25} _{-0.20}	0.008 ^{+0.003} _{-0.003}	-0.25 ^{+0.11} _{-0.08}	0.40 ± 0.02	0.230 ¹¹
Zhang et al. (2018)						
3C 273	8.50 ^{+0.03} _{-0.04}	1.44 ^{+0.06} _{-0.08}	2.01 ^{+0.43} _{-0.45}	-0.41 ^{+0.08} _{-0.08}	1.45 ± 0.03	0.052 ²

NOTES. Columns are as follows: (1) Object name. Discarded object of the analysis are marked † symbol. (2) Black hole mass in units of solar masses considering. (3) Dimensionless accretion rate, see Equation (3). (4) Eddington ratio. (5) Deviations of BLR size from $R_{H\beta} - L_{5100}$ relation. (6) Virial factor anti-correlated with the FWHM of $H\beta$, see Equation (2). F_{var} value. In some cases is specified the origin of the estimation: (1) Hu et al. (2015), (2) Peterson et al. (2004), (3) Bentz et al. (2009), (4) Denney et al. (2010), (5) Bentz et al. (2014), (6) Barth et al. (2013), (7) Pei et al. (2014), (8) Bentz et al. (2016a), (9) Bentz et al. (2016b), (10) Fausnaugh et al. (2017), (11) Lu et al. (2016). F_{var} was estimated for the sources without reference. Columns 2,3,4 and 5 have been computed considering $f_{\text{BLR}}=1$.

Table 3. Observational properties corrected by the effect of dimensionless accretion rate

Object	$\log \dot{M}^c$	$\Delta R_{H\beta, \dot{M}^c}$	τ_{corr} [days]	$D_{L, \text{corr}}$ [Mpc]
(1)	(2)	(3)	(4)	(5)
SEAMBH sample				
Mrk335	$0.19^{+0.34}_{-0.28}$	$-0.28^{+0.10}_{-0.08}$	$26.7^{+8.8}_{-6.5}$	136.1 ± 38.9
Mrk142	$0.81^{+0.99}_{-0.47}$	$-0.46^{+0.28}_{-0.14}$	$18.4^{+21.0}_{-9.8}$	199.7 ± 167.0
IRASF12397	$1.31^{+0.80}_{-0.65}$	$-0.60^{+0.23}_{-0.19}$	$38.6^{+21.9}_{-7.2}$	192.6 ± 72.5
Mrk486	$-0.32^{+0.29}_{-0.14}$	$-0.14^{+0.08}_{-0.04}$	$32.5^{+10.3}_{-3.7}$	271.9 ± 58.5
Mrk382	$0.03^{+0.54}_{-0.49}$	$-0.24^{+0.15}_{-0.14}$	$12.9^{+5.0}_{-3.4}$	180.8 ± 59.1
IRAS04416	$1.52^{+0.91}_{-0.12}$	$-0.66^{+0.26}_{-0.05}$	$60.5^{+63.2}_{-6.4}$	490.6 ± 282.2
MCG06	$-1.59^{+0.36}_{-0.26}$	$0.22^{+0.11}_{-0.08}$	$14.4^{+5.0}_{-2.9}$	327.5 ± 90.1
Mrk493	$0.09^{+0.15}_{-0.23}$	$-0.25^{+0.04}_{-0.07}$	$20.8^{+2.1}_{-4.7}$	268.0 ± 43.9
Mrk1044	$-0.15^{+0.31}_{-0.27}$	$-0.19^{+0.09}_{-0.08}$	$16.1^{+5.1}_{-4.1}$	114.9 ± 32.8
J080101	$1.46^{+1.02}_{-0.29}$	$-0.64^{+0.29}_{-0.09}$	$36.4^{+42.5}_{-11.8}$	602.2 ± 449.9
J081456	$-0.05^{+0.29}_{-0.59}$	$-0.21^{+0.08}_{-0.17}$	$39.7^{+12.6}_{-26.8}$	767.7 ± 380.7
J093922	$1.18^{+0.17}_{-0.46}$	$-0.56^{+0.05}_{-0.13}$	$43.6^{+7.7}_{-23.1}$	1241.0 ± 438.1
J080131	$0.99^{+0.57}_{-0.29}$	$-0.51^{+0.16}_{-0.08}$	$37.0^{+24.3}_{-12.0}$	1159.0 ± 567.9
J085946	$0.51^{+0.48}_{-0.66}$	$-0.37^{+0.14}_{-0.19}$	$82.0^{+45.2}_{-62.0}$	2141.8 ± 1400.3
J102339	$0.31^{+0.69}_{-0.15}$	$-0.32^{+0.20}_{-0.05}$	$51.6^{+41.1}_{-8.1}$	1019.5 ± 485.2
J074352	$1.31^{+0.11}_{-0.09}$	$-0.60^{+0.04}_{-0.04}$	$174.2^{+20.6}_{-16.7}$	1563.7 ± 167.5
J075051	$1.25^{+0.24}_{-0.13}$	$-0.58^{+0.07}_{-0.05}$	$254.6^{+71.5}_{-37.8}$	4086.4 ± 877.5
J075101	$0.39^{+0.22}_{-0.18}$	$-0.34^{+0.06}_{-0.05}$	$66.2^{+15.8}_{-12.6}$	968.3 ± 208.2
J075949	$-0.05^{+0.66}_{-0.39}$	$-0.21^{+0.19}_{-0.11}$	$71.8^{+54.3}_{-31.2}$	1803.4 ± 1072.6
J081441	$0.07^{+0.36}_{-0.26}$	$-0.25^{+0.10}_{-0.08}$	$44.7^{+18.4}_{-13.3}$	1264.3 ± 447.5
J083553	$1.43^{+0.38}_{-0.38}$	$-0.63^{+0.11}_{-0.11}$	$53.4^{+23.3}_{-23.3}$	1107.6 ± 482.4
J084533	$1.44^{+0.29}_{-0.23}$	$-0.64^{+0.09}_{-0.07}$	$78.5^{+26.1}_{-20.5}$	2307.1 ± 683.8
J093302	$0.85^{+0.26}_{-0.28}$	$-0.47^{+0.08}_{-0.08}$	$55.9^{+11.2}_{-12.7}$	1144.7 ± 244.0
J100402	$2.10^{+1.17}_{-0.11}$	$-0.82^{+0.33}_{-0.05}$	$214.2^{+289.5}_{-28.0}$	2182.5 ± 1616.9
J101000	$1.02^{+0.74}_{-0.24}$	$-0.52^{+0.21}_{-0.07}$	$91.0^{+77.2}_{-25.0}$	1677.6 ± 941.8
SDSS sample				
J140812	$-1.00^{+0.27}_{-0.32}$	$0.06^{+0.08}_{-0.09}$	$9.2^{+0.9}_{-1.9}$	450.4 ± 68.6
J141923	$-0.87^{+0.06}_{-0.11}$	$0.02^{+0.03}_{-0.04}$	$11.3^{+0.7}_{-1.4}$	767.1 ± 71.5
J140759	$-0.63^{+0.70}_{-0.35}$	$-0.05^{+0.20}_{-0.10}$	$18.3^{+14.7}_{-7.4}$	843.3 ± 509.6
J141729	$-0.78^{+0.90}_{-0.34}$	$-0.01^{+0.26}_{-0.10}$	$5.6^{+5.8}_{-2.1}$	513.3 ± 364.0
J141645.15	$-0.66^{+0.26}_{-0.25}$	$-0.04^{+0.08}_{-0.07}$	$5.5^{+1.7}_{-1.5}$	571.3 ± 165.7
J142135	$0.58^{+0.21}_{-0.21}$	$-0.39^{+0.06}_{-0.06}$	$9.6^{+2.2}_{-2.2}$	756.9 ± 174.7
J141625	$0.05^{+0.19}_{-0.27}$	$-0.24^{+0.06}_{-0.08}$	$26.3^{+5.6}_{-8.0}$	1252.6 ± 323.5
J142103	$-1.72^{+0.06}_{-0.06}$	$0.26^{+0.04}_{-0.04}$	$41.4^{+1.8}_{-1.8}$	2868.9 ± 124.0
J142038	$-1.36^{+0.16}_{-0.20}$	$0.16^{+0.05}_{-0.06}$	$17.5^{+3.3}_{-4.0}$	1503.1 ± 310.2
J142043	$-0.15^{+0.08}_{-0.10}$	$-0.19^{+0.03}_{-0.03}$	$9.1^{+0.6}_{-0.9}$	1096.8 ± 93.0
J141041	$-0.74^{+0.17}_{-0.10}$	$-0.02^{+0.05}_{-0.03}$	$22.8^{+4.4}_{-2.5}$	1825.9 ± 275.1
J141318	$-0.21^{+0.05}_{-0.13}$	$-0.17^{+0.02}_{-0.04}$	$29.4^{+1.6}_{-4.4}$	2080.1 ± 213.2
J141955	$-0.98^{+0.49}_{-0.40}$	$0.05^{+0.14}_{-0.11}$	$9.5^{+5.0}_{-3.9}$	1498.1 ± 700.0
J141645.58	$0.46^{+0.26}_{-0.15}$	$-0.36^{+0.08}_{-0.05}$	$19.5^{+5.7}_{-3.2}$	2352.9 ± 539.8
J141324	$-0.83^{+0.37}_{-0.20}$	$0.01^{+0.11}_{-0.06}$	$25.1^{+10.7}_{-5.7}$	2317.8 ± 759.0
J141214	$0.60^{+0.29}_{-0.35}$	$-0.40^{+0.08}_{-0.10}$	$53.5^{+10.5}_{-16.0}$	2950.6 ± 730.8

J140518	-0.26 ^{+0.31} _{-0.17}	-0.16 ^{+0.09} _{-0.05}	59.5 ^{+21.2} _{-11.9}	3619.4 \pm 1004.9
J141018	-0.73 ^{+0.21} _{-0.28}	-0.02 ^{+0.06} _{-0.08}	17.0 ^{+3.0} _{-4.7}	2464.1 \pm 562.8
J141123	0.31 ^{+0.10} _{-0.06}	-0.32 ^{+0.03} _{-0.02}	27.0 ^{+2.9} _{-1.7}	2101.4 \pm 177.8
J142039	-0.10 ^{+0.06} _{-0.13}	-0.20 ^{+0.02} _{-0.04}	32.8 ^{+1.4} _{-4.8}	2535.0 \pm 238.8
J141724	0.15 ^{+1.07} _{-0.23}	-0.27 ^{+0.30} _{-0.07}	18.9 ^{+23.4} _{-5.0}	1763.9 \pm 1327.3
J141004	-0.53 ^{+0.08} _{-0.08}	-0.08 ^{+0.03} _{-0.03}	64.2 ^{+5.0} _{-4.8}	5113.1 \pm 391.8
J141706	1.24 ^{+0.53} _{-0.25}	-0.58 ^{+0.15} _{-0.08}	39.4 ^{+23.9} _{-11.4}	3318.1 \pm 1483.7
J142010	-0.01 ^{+0.43} _{-0.35}	-0.22 ^{+0.12} _{-0.10}	21.5 ^{+9.6} _{-7.5}	2096.5 \pm 835.3
J141712	-0.59 ^{+0.39} _{-0.41}	-0.06 ^{+0.11} _{-0.12}	14.4 ^{+2.1} _{-3.0}	3916.2 \pm 689.3
J141115	-0.44 ^{+0.20} _{-0.05}	-0.10 ^{+0.06} _{-0.02}	62.4 ^{+14.1} _{-2.5}	4955.6 \pm 661.1
J141112	0.20 ^{+0.11} _{-0.09}	-0.28 ^{+0.04} _{-0.03}	39.3 ^{+4.8} _{-3.8}	4003.1 \pm 441.5
J141417	-1.27 ^{+0.30} _{-0.38}	0.13 ^{+0.09} _{-0.11}	11.5 ^{+2.4} _{-3.8}	2803.4 \pm 745.8
J141031	-0.61 ^{+0.07} _{-0.26}	-0.06 ^{+0.03} _{-0.08}	40.6 ^{+1.2} _{-11.7}	4857.2 \pm 773.3
J141941	0.44 ^{+0.12} _{-0.24}	-0.35 ^{+0.04} _{-0.07}	68.4 ^{+8.8} _{-18.7}	4947.3 \pm 992.8
J141135	0.27 ^{+0.43} _{-0.37}	-0.30 ^{+0.12} _{-0.11}	35.5 ^{+17.4} _{-14.9}	4509.7 \pm 2049.9
J140904	-0.23 ^{+0.68} _{-0.40}	-0.16 ^{+0.19} _{-0.12}	16.9 ^{+12.5} _{-6.7}	1923.8 \pm 1094.6
J142052	1.87 ^{+0.10} _{-0.07}	-0.76 ^{+0.05} _{-0.04}	68.2 ^{+7.5} _{-5.7}	2810.9 \pm 271.8
J141147	1.18 ^{+0.21} _{-0.20}	-0.56 ^{+0.07} _{-0.06}	23.4 ^{+5.5} _{-5.1}	3188.0 \pm 722.4
J141532	0.38 ^{+0.33} _{-0.29}	-0.34 ^{+0.09} _{-0.08}	57.4 ^{+21.4} _{-19.0}	7326.8 \pm 2585.2
J142023	0.76 ^{+0.33} _{-0.40}	-0.44 ^{+0.10} _{-0.12}	23.7 ^{+8.9} _{-10.9}	2827.5 \pm 1181.0
J142049	-0.40 ^{+0.18} _{-0.18}	-0.11 ^{+0.06} _{-0.06}	59.9 ^{+12.4} _{-12.4}	5688.3 \pm 1174.8
J142112	0.46 ^{+0.26} _{-0.23}	-0.36 ^{+0.08} _{-0.07}	32.4 ^{+8.5} _{-6.9}	4128.8 \pm 974.1
J141606	0.12 ^{+0.32} _{-0.42}	-0.26 ^{+0.09} _{-0.12}	58.7 ^{+21.3} _{-28.4}	4298.4 \pm 1820.2
J141859	0.95 ^{+0.24} _{-0.30}	-0.50 ^{+0.07} _{-0.09}	64.0 ^{+17.6} _{-22.0}	4366.7 \pm 1348.6
J141952	-0.77 ^{+0.17} _{-0.16}	-0.01 ^{+0.05} _{-0.05}	33.6 ^{+5.7} _{-5.2}	4911.1 \pm 798.6
J142417	-0.01 ^{+0.22} _{-0.23}	-0.22 ^{+0.06} _{-0.07}	60.9 ^{+7.6} _{-9.2}	10753.6 \pm 1481.3

Bentz collection

PG0026+129	0.34 ^{+0.61} _{-0.62}	-0.32 ^{+0.17} _{-0.18}	234.4 ^{+50.9} _{-59.8}	1761.2 \pm 415.8
PG0052+251	-0.36 ^{+0.30} _{-0.30}	-0.13 ^{+0.09} _{-0.09}	120.2 ^{+32.8} _{-32.3}	1191.0 \pm 322.3
Fairall9	-0.54 ^{+0.27} _{-0.30}	-0.08 ^{+0.08} _{-0.09}	20.8 ^{+3.8} _{-5.1}	151.1 \pm 32.6
Mrk590	-0.78 ^{+0.74} _{-0.73}	-0.01 ^{+0.21} _{-0.21}	26.0 ^{+6.6} _{-5.4}	180.4 \pm 41.6
3C120	-0.09 ^{+0.53} _{-0.50}	-0.20 ^{+0.15} _{-0.14}	41.9 ^{+13.9} _{-10.6}	206.4 \pm 60.3
Ark120	-1.24 ^{+0.44} _{-0.44}	0.12 ^{+0.13} _{-0.13}	29.7 ^{+6.4} _{-5.9}	171.3 \pm 35.3
Mrk79	-0.64 ^{+0.72} _{-0.71}	-0.05 ^{+0.20} _{-0.20}	17.3 ^{+6.0} _{-5.4}	82.4 \pm 27.2
PG0804+761	-0.11 ^{+0.85} _{-0.85}	-0.20 ^{+0.24} _{-0.24}	231.7 ^{+29.7} _{-29.8}	1278.3 \pm 164.1
Mrk110	-0.25 ^{+1.13} _{-1.12}	-0.16 ^{+0.32} _{-0.32}	36.7 ^{+12.8} _{-10.3}	286.4 \pm 90.1
PG0953+414	0.001 ^{+0.30} _{-0.30}	-0.23 ^{+0.09} _{-0.09}	253.8 ^{+36.5} _{-38.2}	2587.7 \pm 381.0
NGC3227	-1.36 ^{+0.25} _{-0.25}	0.16 ^{+0.08} _{-0.08}	2.7 ^{+0.6} _{-0.6}	11.9 \pm 2.5
NGC3516	-1.77 ^{+0.32} _{-0.33}	0.27 ^{+0.10} _{-0.10}	6.2 ^{+0.5} _{-0.8}	33.3 \pm 3.6
SBS1116+583A	-1.07 ^{+0.75} _{-0.74}	0.08 ^{+0.21} _{-0.21}	1.9 ^{+0.5} _{-0.4}	68.9 \pm 16.5
Arp151	-0.63 ^{+0.22} _{-0.25}	-0.05 ^{+0.07} _{-0.07}	4.5 ^{+0.6} _{-0.8}	74.3 \pm 11.1
NGC3783	-1.63 ^{+0.52} _{-0.48}	0.23 ^{+0.15} _{-0.14}	6.0 ^{+1.9} _{-1.3}	46.3 \pm 12.7
Mrk1310	-0.67 ^{+0.41} _{-0.41}	-0.04 ^{+0.12} _{-0.12}	4.0 ^{+0.7} _{-0.7}	85.7 \pm 13.9
NGC4051	-0.45 ^{+0.44} _{-0.38}	-0.10 ^{+0.13} _{-0.11}	2.6 ^{+1.1} _{-0.9}	8.7 \pm 3.3
NGC4151	-2.25 ^{+0.47} _{-0.46}	0.41 ^{+0.14} _{-0.14}	2.6 ^{+0.4} _{-0.3}	10.2 \pm 1.5
Mrk202	-0.42 ^{+0.65} _{-0.53}	-0.11 ^{+0.19} _{-0.15}	3.9 ^{+2.2} _{-1.4}	89.5 \pm 41.8
NGC4253	-0.23 ^{+3.05} _{-3.05}	-0.16 ^{+0.86} _{-0.86}	9.0 ^{+2.3} _{-1.7}	89.8 \pm 20.3
PG1229+204	-1.13 ^{+0.66} _{-0.40}	0.09 ^{+0.19} _{-0.12}	30.6 ^{+22.4} _{-12.4}	419.3 \pm 237.9
NGC4593	-0.95 ^{+0.64} _{-0.63}	0.04 ^{+0.18} _{-0.18}	3.6 ^{+0.7} _{-0.6}	23.6 \pm 4.4
NGC4748	-0.42 ^{+0.42} _{-0.49}	-0.11 ^{+0.12} _{-0.14}	7.1 ^{+2.1} _{-2.9}	82.8 \pm 28.8

PG1307+085	-0.58 ^{+0.36} _{-0.44}	-0.07 ^{+0.10} _{-0.13}	122.7 ^{+41.8} _{-54.1}	1165.7 \pm 455.9
Mrk279	-0.40 ^{+0.31} _{-0.31}	-0.11 ^{+0.09} _{-0.09}	21.8 ^{+5.1} _{-5.1}	137.2 \pm 32.0
PG1411+442	-0.61 ^{+0.52} _{-0.52}	-0.06 ^{+0.15} _{-0.15}	141.3 ^{+69.3} _{-70.1}	1038.8 \pm 512.7
PG1426+015	-0.97 ^{+0.50} _{-0.53}	0.05 ^{+0.14} _{-0.15}	85.1 ^{+26.8} _{-33.2}	559.4 \pm 197.3
Mrk817	-0.64 ^{+0.74} _{-0.67}	-0.05 ^{+0.21} _{-0.19}	22.2 ^{+11.0} _{-7.5}	143.1 \pm 59.7
Mrk290	-0.81 ^{+0.16} _{-0.15}	0.001 ^{+0.05} _{-0.05}	8.7 ^{+1.2} _{-1.0}	101.7 \pm 13.0
PG1613+658	-0.17 ^{+0.56} _{-0.56}	-0.18 ^{+0.16} _{-0.16}	60.8 ^{+22.7} _{-23.0}	515.3 \pm 194.1
PG1617+175	-0.87 ^{+0.56} _{-0.59}	0.02 ^{+0.16} _{-0.17}	68.3 ^{+28.3} _{-32.2}	773.7 \pm 342.5
PG1700+518	0.50 ^{+0.76} _{-0.76}	-0.37 ^{+0.22} _{-0.21}	590.8 ^{+107.8} _{-91.2}	4894.0 \pm 824.1
3C390.3	-0.97 ^{+1.09} _{-1.00}	0.05 ^{+0.31} _{-0.28}	40.0 ^{+24.9} _{-15.3}	207.4 \pm 104.3
NGC6814	-1.95 ^{+0.48} _{-0.48}	0.32 ^{+0.14} _{-0.14}	3.1 ^{+0.4} _{-0.4}	20.0 \pm 2.7
Mrk509	-0.87 ^{+0.12} _{-0.12}	0.02 ^{+0.04} _{-0.04}	76.5 ^{+5.9} _{-5.2}	312.7 \pm 22.6
PG2130+099	1.17 ^{+0.15} _{-0.15}	-0.56 ^{+0.05} _{-0.05}	34.9 ^{+4.4} _{-4.4}	266.8 \pm 33.4
NGC7469	0.51 ^{+0.35} _{-0.25}	-0.37 ^{+0.10} _{-0.07}	25.5 ^{+8.0} _{-3.1}	106.8 \pm 23.2
PG1211+143	0.01 ^{+0.27} _{-0.41}	-0.23 ^{+0.08} _{-0.12}	159.7 ^{+43.6} _{-71.7}	868.9 \pm 313.6
PG0844+349	0.03 ^{+0.47} _{-0.46}	-0.24 ^{+0.13} _{-0.13}	55.8 ^{+23.7} _{-23.2}	426.6 \pm 179.0
NGC5273	-2.12 ^{+0.55} _{-0.69}	0.37 ^{+0.16} _{-0.20}	0.9 ^{+0.5} _{-0.7}	9.4 \pm 6.0
Mrk1511	-0.43 ^{+0.18} _{-0.17}	-0.11 ^{+0.05} _{-0.05}	7.3 ^{+1.1} _{-1.0}	97.5 \pm 14.7
KA1858-4850	-0.05 ^{+0.17} _{-0.19}	-0.21 ^{+0.05} _{-0.06}	22.1 ^{+3.3} _{-3.8}	516.2 \pm 82.6
MCG6-30-15	-1.94 ^{+0.67} _{-0.66}	0.32 ^{+0.19} _{-0.19}	2.7 ^{+0.9} _{-0.8}	48.5 \pm 14.7
UGC06728	-0.23 ^{+0.46} _{-0.52}	-0.16 ^{+0.13} _{-0.15}	2.0 ^{+1.0} _{-1.2}	21.1 \pm 11.3
MCG+08-11-011	-0.14 ^{+0.17} _{-0.17}	-0.19 ^{+0.05} _{-0.05}	24.3 ^{+0.8} _{-0.8}	164.0 \pm 5.3
NGC2617	-1.10 ^{+0.33} _{-0.36}	0.08 ^{+0.10} _{-0.11}	3.5 ^{+0.9} _{-1.1}	34.0 \pm 9.7
3C382	-1.02 ^{+0.28} _{-0.17}	0.06 ^{+0.08} _{-0.06}	35.1 ^{+6.9} _{-3.2}	376.6 \pm 54.6
Mrk374	-0.16 ^{+0.35} _{-0.20}	-0.18 ^{+0.10} _{-0.06}	22.5 ^{+8.8} _{-5.0}	189.7 \pm 58.3
Lu et al. (2016)				
NGC5548	-1.19 ^{+0.25} _{-0.20}	0.11 ^{+0.08} _{-0.06}	5.6 ^{+1.0} _{-0.3}	34.7 \pm 4.1
Zhang et al. (2018)				
3C 273	1.12 ^{+0.07} _{-0.08}	-0.54 ^{+0.03} _{-0.03}	514.1 ^{+29.1} _{-42.4}	1380.8 \pm 96.0

NOTES. Columns are as follows: (1) Object name. (2) Dimensionless accretion rate. (3) Deviation of the expected $R_{H\beta} - L_{5100}$ estimated from the Equation (10). (4) Time delay corrected by the dimensionless accretion rate in unit of days. (6) Luminosity distance in units of Mpc.